Lithos 155 (2012) 67–80

Contents lists available at SciVerse ScienceDirect

Lithos

journal homepage: www.elsevier.com/locate/lithos

Metasomatized lithosphere–asthenosphere interaction during slab roll-back: Evidence from Late Carboniferous gabbros in the Luotuogou area, Central Tianshan

Gong-Jian Tang [a,b], Qiang Wang [a,*], Derek A. Wyman [c], Zheng-Xiang Li [d], Yi-Gang Xu [a], Zhen-Hua Zhao [a]

[a] State Key Laboratory of Isotope Geochemistry, Guangzhou Institute of Geochemistry, Chinese Academy of Sciences, Guangzhou 510640, PR China
[b] Graduate University of Chinese Academy of Sciences, Beijing 100049, PR China
[c] School of Geosciences, The University of Sydney, NSW 2006, Australia
[d] ARC Centre of Excellence for Core to Crust Fluid Systems (CCFS) and The Institute for Geoscience Research (TIGeR), Department of Applied Geology, Curtin University, GPO Box U1987, Perth,WA 6845, Australia

ARTICLE INFO

Article history:
Received 14 May 2012
Accepted 18 August 2012
Available online 29 August 2012

Keywords:
Gabbro
Clinopyroxene
Lithosphere–asthenosphere interaction
Slab roll-back
Carboniferous
Tianshan Orogen

ABSTRACT

Late Carboniferous igneous rocks are widespread in the western Tianshan, but the tectonic settings for these rocks remain controversial. We report a plagioclase $^{40}Ar/^{39}Ar$ age, and geochemical, Sr–Nd isotope and LA–ICPMS clinopyroxene trace element data for gabbros in the Luotuogou region. The tholeiitic Luotuogou gabbros give a Late Carboniferous (312±1 Ma) $^{40}Ar/^{39}Ar$ age and are characterized by high and variable $\varepsilon_{Nd}(t)$ values ranging from +3.7 to +7.8. They have geochemical features of both intra-plate and island arc magmatic rocks, i.e., relatively high TiO_2 (0.6–2.2 wt.%), Nb (4.2–24 ppm) and Zr (51.4–283 ppm) contents combined with variable and slightly high Nb/La ratios (0.24–1.8, mostly > 0.7), and negative to positive Nb anomalies. The gabbros contain zoned clinopyroxenes, with Mg- and Cr-rich cores. Their parental magmas, as calculated using trace element data from Cr-rich (>3000 ppm) clinopyroxene cores and clinopyroxene/basaltic liquid partition coefficients, show enrichments in incompatible elements, and prominent negative to slightly positive Nb anomalies, indicative of the influence of subduction-related compositions in their mantle source. These features indicate that the Luotuogou gabbros were most likely formed by interactions between asthenospheric and metasomatized lithospheric mantle. They were most plausibly formed by mixing between the asthenospheric mantle-derived and metasomatized lithosphere mantle-derived melts. Mixing was the result of asthenosphere upwelling triggered by roll-back of the subducted Paleo-Junggar Oceanic Plate rather than mantle plume-related rifting or post-collisional break-off during the Late Carboniferous.

1. Introduction

Continental basaltic magmas record critical information regarding the chemical composition of the sub-continental mantle and regional tectonic evolution. Several distinct mantle components can contribute to continental basalts, such as subcontinental lithospheric mantle, plume-related OIB (oceanic island basalt)-type mantle sources, or depleted MORB (middle oceanic ridge basalt)-type asthenosphere mantle (Garfunkel, 2008; Saunders, 2005). Popular tectonic models for continental volcanism include decompressional melting as a result of lithospheric mantle removal (detachment) and upwelling asthenosphere mantle (Hoernle et al., 2006; Timm et al., 2009), lithosphere extension induced by continental rifting and breakup (McKenzie and Bickle, 1988), high temperature melting of mantle owing to elevated mantle temperature by deep-seated mantle plume head impinging on the lithosphere (Campbell and Griffiths, 1990), and the roll-back and/or foundering of flat-subducted oceanic plateaus or aseismic ridges (Coney and Reynolds, 1977; Li and Li, 2007). Identifying the primary magmas for continental basaltic magmas thus has the potential of deciphering their petrogenesis and related tectonic processes.

However, continental basaltic magmas generally show variable chemical compositions due to contamination by continental crustal components or fractionation during their ascent (Dorais and Tubrett, 2008). One approach that overcomes these problems uses clinopyroxene chemical composition and basaltic liquid partition coefficients to model the most primitive liquids to have been in equilibrium with the clinopyroxenes (Tribuzio et al., 2008, 2009). The results are then compared with various mantle-derived basaltic magmas to draw inferences about the primary magma compositions (Chen et al., 2009; Dorais and Tubrett, 2008; Tribuzio et al., 2008, 2009).

The Tianshan Orogen, extends from west to east for over 2500 km through Uzbekistan, Tajikistan, Kyrgyzstan, and Kazakhstan to Xinjiang in northwestern China (Fig. 1a). It is a major part of the southwestern Central Asian Orogenic Belt (CAOB) (Jahn et al., 2000; Sengör et al., 1993; Windley et al., 2007; Xiao et al., 2004). It mainly consists of microcontinents, ophiolite and mélange belts, continental island arcs, and remnant seamounts and oceanic plateaus, accreted

* Corresponding author at. Tel.: +86 20 85290277; fax: +86 20 85290130.
E-mail address: wqiang@gig.ac.cn (Q. Wang).

0024-4937/$ – see front matter © 2012 Elsevier B.V. All rights reserved.
http://dx.doi.org/10.1016/j.lithos.2012.08.015

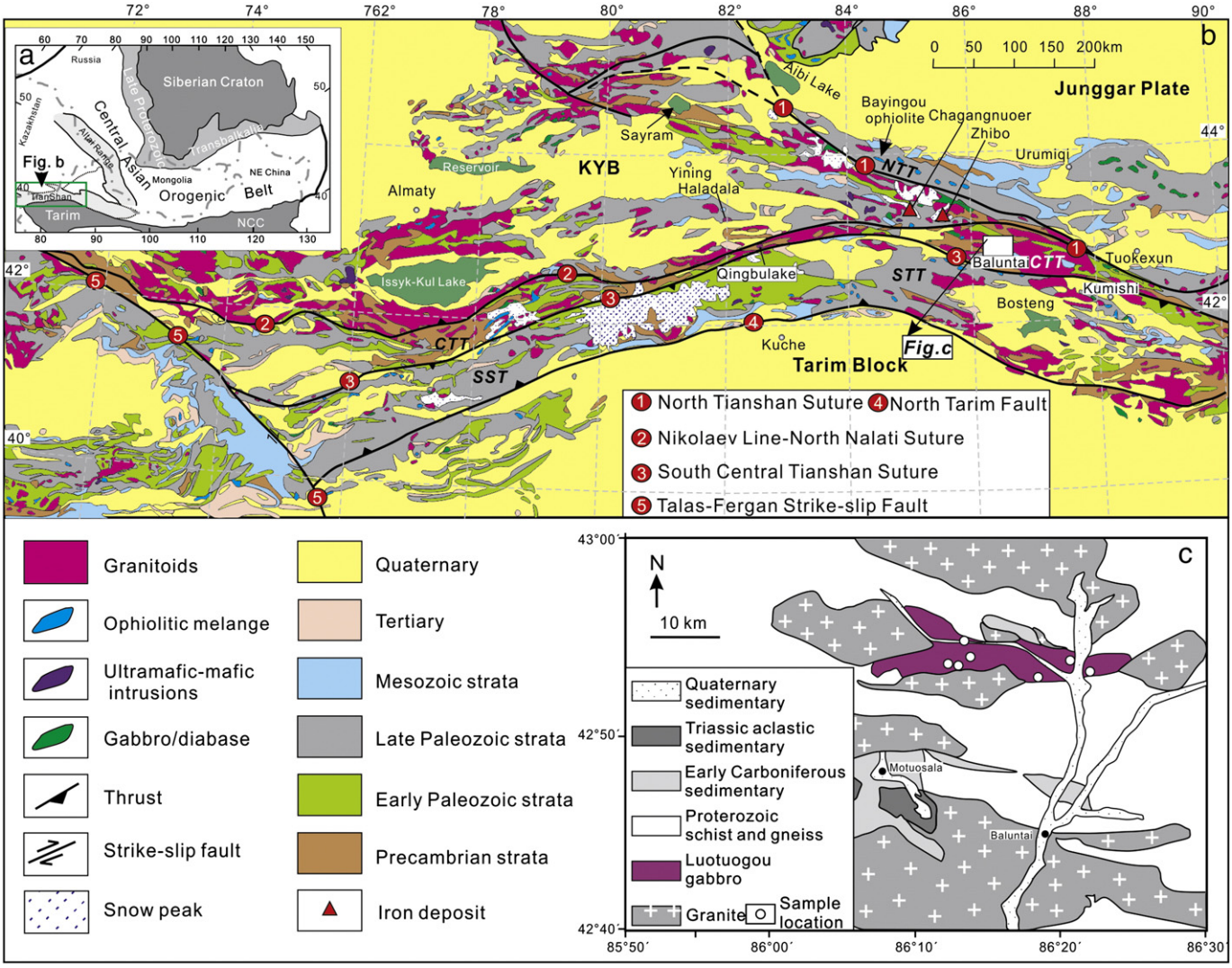

Fig. 1. (a) Simplified tectonic divisions of the CAOB (Jahn et al., 2000), (b) geological map of the western Tianshan orogen (Gao et al., 2009) and (c) geological map showing the occurrence of the Luotuogou gabbros. "Snow peak" in Fig. 1a refers to the area with generally high altitude and covered with snow all the year round. NTT, Northern Tianshan Terrane, CTT, Central Tianshan Terrane, KYB, Kazakhstan–Yili Block.

together between the Neoproterozoic and late Paleozoic (Gao et al., 1998; Xiao et al., 2008). Thus, the Tianshan Orogen is a key area for understanding the tectonic evolution and Phanerozoic continental growth of the CAOB.

There are voluminous Silurian–Permian granitoids in the Central Tianshan Terrane, but mafic rocks are rare and most formed during the Late Carboniferous. The origin of these mafic rocks has been a matter of debate in three competing models: 1) mantle plume or crustal rifting (Che and Liu, 1996; Xia et al., 2004b, 2008), which predicts a dominant role for an upwelling deep-seated mantle plume impinging on the lithosphere (Xia et al., 2004b, 2008); 2) an island arc model, which suggests a subduction of the Paleo-Tianshan Oceanic Plate (Wang et al., 2007; Zhou et al., 2004; Zhu et al., 2005, 2009); or 3) a post-collisional model that invokes slab break-off and subsequent asthenospheric upwelling after the collision between the Junggar plate and the Yili terrane (e.g., Han et al., 2010; Yuan et al., 2010). In this study, we determined plagioclase $^{40}Ar/^{39}Ar$ ages and undertook whole rock geochemical and Sr–Nd isotope analyses, electron microprobe analyses of clinopyroxene major element compositions and LA–ICPMS clinopyroxene trace element analyses for the Luotuogou gabbros north of Baluntai town in the Central Tianshan Terrane (Fig. 1). The combined results are used to reveal the mantle source and petrogenesis of the gabbros in order to shed new light on the tectonic evolution of the Tianshan Orogen.

2. Geological background

The Chinese Tianshan, located between the Junggar plate to the north and the Tarim Block to the south, is a ca 300 km-wide Paleozoic collisional orogenic collage (Fig. 1b). It experienced a complex evolutionary history involving Paleozoic subduction and collision, Mesozoic erosion, and Cenozoic thrusting and uplift as a consequence of the India–Eurasia collision that has continued to the present (Allen et al., 1993; Gao et al., 1998; Windley et al., 1990; Xiao et al., 2008). The orogen can be subdivided into several geological domains, which are from north to south, the Northern Tianshan Terrane, the Kazakhstan–Yili Block, the Central Tianshan Terrane (CTT) and the South Tianshan Terrane (Gao et al., 2009). The North Tianshan Terrane represents a Late Paleozoic continental magmatic arc related to south-directed subduction of the Junggar Oceanic Plate during the Late Ordovician–Early Permian (Gao et al., 1998). It is characterized by the presence of Late Devonian–Carboniferous sedimentary sequences and abundant calc-alkaline volcanic and intrusive rocks. The

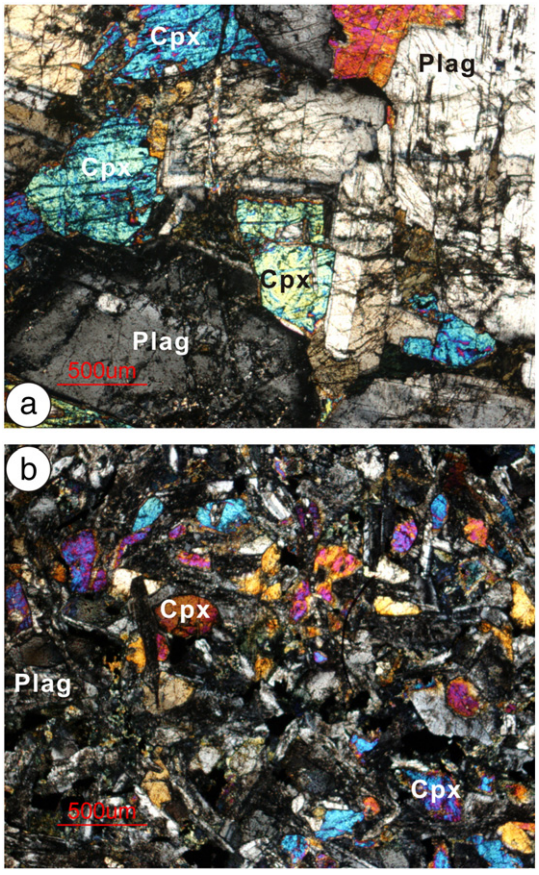

Fig. 2. Photomicrographs showing the main textures and mineral assemblages in the Luotuogou gabbros. Cpx, clinopyroxene; Plag, plagioclase.

Kazakhstan–Yili Block is a microcontinent with a Precambrian basement (Allen et al., 1993; Gao et al., 1998). The South Tianshan Terrane resulted from the collision between the Tarim Block and the Kazakhstan–Yili Block during the Late Paleozoic (Gao et al., 2009).

The CTT is separated from the South Tianshan Terrane by the South Central Tianshan Suture defined by ophiolites with ages ranging from the Early Ordovician to Early Carboniferous (Xiao et al., 2008). These include the Changwuazi ophiolite that has a pyroxene $^{40}Ar/^{39}Ar$ plateau age of 439±27 Ma (Hao and Liu, 1993), and the Yushugou and Tonghuagou ophiolites in the Kumishi region where plagiogranite and anorthosite yielded SHRIMP zircon U–Pb ages of 435±3 Ma and 439±2 Ma, respectively (Yang et al., 2011). The "Nikolaev Line" or North Nalati Suture (Qian et al., 2009) separates the CTT and the Kazakhstan–Yili Block (Gao et al., 2009). Mid-ocean ridge basalts with a SHRIMP U–Pb zircon age of 516±7 Ma have been reported along the southern margin of the Kazakhstan–Yili Block (Qian et al., 2009).

The CTT is underlain by Proterozoic metamorphic basement, mainly exposed in the Baluntai area. The basement mainly consists of sillimanite–biotite–quartz schists, garnet–plagioclase–granulites, gneisses, amphibolites, migmatites and marbles. Proterozoic granite gneisses have zircon U–Pb ages ranging from 948±8 to 926±8 Ma (Chen et al., 2009; Hu et al., 2010). Paleozoic (480–275 Ma) granitoids are widely distributed in this terrane (Dong et al., 2011; Gao et al., 2009, 2011; Shi et al., 2007; Yang et al., 2006). Late Devonian to Late Carboniferous (>361–313 Ma, SHRIMP U–Pb zircon age) island-arc type volcanic and volcaniclastic rocks disconformably overlie Late Silurian volcanics or the Proterozoic basement (Tang et al., 2010; Zhu et al., 2009).

Late Carboniferous mafic intrusive and contemporaneous mafic volcanic rocks are very abundant in the western Tianshan, i.e., 306–308 Ma mafic–ultramafic intrusions in the Tekes Haladala area of the CTT (Xue and Zhu, 2009; Zhu et al., 2010), 305–300 Ma basalts from the Chagangnuoer and Zhibo iron deposits (Jiang et al., 2012), and ~324–309 Ma basalts in the Yuximolegai and Laerdundaban areas (Niu et al., 2010; Zhu et al., 2009).

The Luotuogou gabbroic pluton intrudes the Proterozoic metamorphic basement north of Baluntai town (Fig. 1b) and is the biggest mafic intrusion in the CTT. The Luotuogou intrusion is distinctly zoned, consisting of fine-grained gabbros in the thin margin (50 to 200 m width) and coarse- to medium-grained gabbros in the interior of the major body. The main mineral phases are clinopyroxene and plagioclase, plus minor amphibole and accessory minerals including Fe–Ti oxides and apatite. Some pyroxene crystals are replaced by amphibole or chlorite along the rims, with clinopyroxene cores being locally preserved (Fig. 2).

3. Analytical methods

Mineral major element analyses were carried out at the State Key Laboratory of Isotope Geochemistry, Guangzhou Institute of Geochemistry, Chinese Academy of Sciences (GIG-CAS) using a JXA-8100 electron microprobe. An accelerating voltage of 15 kV, a specimen current of 3.0×10^{-8} A, and a beam size of 1–2 μm were employed. The analytical procedures were described in detail in Huang et al. (2007), and the analytical errors are generally less than 2%.

In-situ trace element analysis of clinopyroxene was carried out using the laser-ablation (LA)–ICP-MS technique using an Agilent 7500a ICP-MS system coupled with a GeoLas193 nm ArF-excimer laser sampler at GIG-CAS. A spot size of 78 μm and repetition rate of 8 Hz were applied during the analysis. Calibration was carried out externally using NIST SRM 610 with Ca as an internal standard to correct for any drift.

Table 1
Plagioclase $^{40}Ar/^{39}Ar$ dating results of the Luotuogou gabbro.

T (°C)	$^{40}Ar/^{36}Ar$	$^{39}Ar/^{36}Ar$	$^{37}Ar/^{39}Ar$	F	^{39}Ar ($\times10^{-12}$ mol)	^{39}Ar (%)	$^{40}Ar^*$ (%)	Age (Ma)	1σ (Ma)
350	1451.375	22.215	0.0142	52.0309	0.0588	1.04	79.63	348.1	5.2
480	1806.235	32.015	0.0149	47.1888	0.1328	2.35	83.63	318.4	2.0
600	3862.745	79.199	0.0049	45.0415	0.4285	7.66	92.33	305.1	0.7
750	4518.349	90.171	0.0079	46.8314	0.4890	8.65	93.44	316.2	0.8
850	5596.591	112.780	0.0020	47.0039	0.8123	14.37	94.70	317.3	0.5
980	7859.043	162.627	0.0026	46.5084	1.2227	21.63	96.22	314.2	0.4
1120	10,368.421	220.476	0.0024	45.6871	1.3256	23.45	97.13	309.1	0.3
1200	10,478.794	225.267	0.0033	45.2055	0.9661	17.09	97.16	306.1	0.4
1250	11,726.463	244.081	0.0118	46.8327	0.1402	2.48	97.46	316.2	3.0
1350	13,555.602	278.407	0.0214	48.1431	0.0769	1.36	97.80	324.3	4.2

J=0.004091; total sample weight=0.1122 g; Tp=311.89±0.65 Ma; Tf=315.27±0.70 Ma; Tiso=309.16±6.18 Ma.
Tp — Plateau age; Tf — total fusion age; Tiso — isochron.

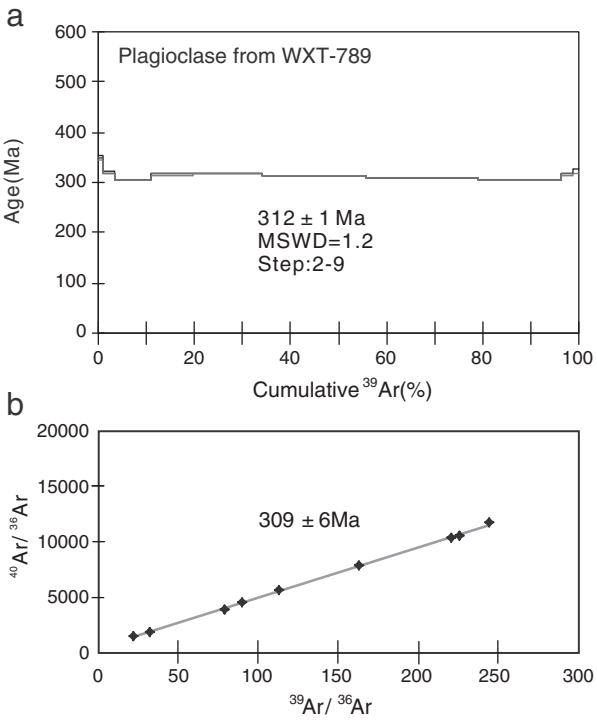

Fig. 3. ^{40}Ar/^{39}Ar geochronological results for plagioclase from the Luotuogou gabbros.

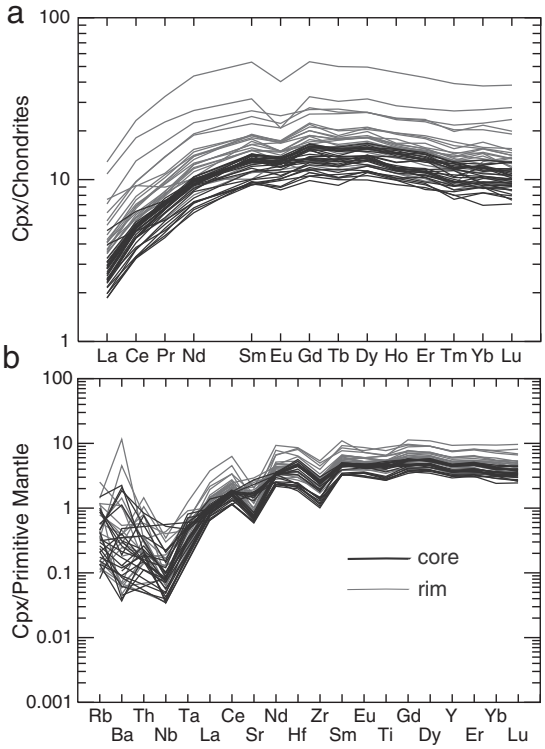

Fig. 5. Chondrite-normalized REE patterns and primitive mantle-normalized multi-element patterns for clinopyroxenes of the Luotuogou gabbros.
Chondrite and primitive mantle normalizing values are from Sun and McDonough (1989).

Repeated analyses of the USGS rock standards BHVO-2G and BCR-2G indicate that both precision and accuracy are better than 4% for most elements analyzed. Analytical details are as in Liu et al. (2008).

Major element oxides were determined by standard X-ray fluorescence (XRF) at GIG-CAS. A detailed description of this analytical method was provided by Li et al. (2006). Trace elements were analyzed by inductively coupled plasma mass spectrometry (ICP-MS), using a Perkin-Elmer Sciex ELAN 6000 instrument at GIG-CAS. Analytical

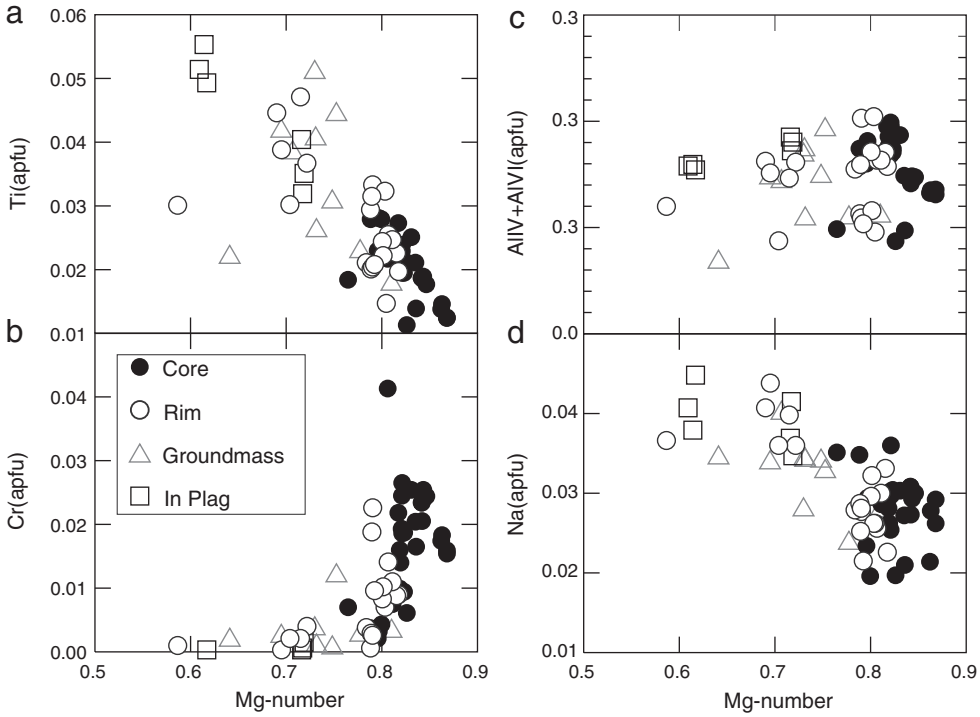

Fig. 4. Chemical variations in Luotuogou gabbro clinopyroxenes. Apfu stands for atoms per formula unit. "In Plag" refers to those clinopyroxenes in plagioclase phenocrysts from coarse-grained gabbros.

Table 2
Major (wt.%) and trace element (ppm) composition of the Luotuogou samples.

Samples	wxt772	wxt773	wxt774	wxt775	wxt776	wxt779	wxt780	wxt781	wxt782	wxt783	wxt784	wxt785	wxt786	wxt787	wxt789
SiO_2	50.81	48.93	49.53	49.85	52.04	48.92	49.93	48.87	49.28	49.52	48.36	48.11	49.20	48.01	48.55
TiO_2	1.66	1.16	1.57	1.53	2.07	1.39	1.46	1.82	2.14	1.31	1.12	0.66	1.55	1.92	0.85
Al_2O_3	16.78	17.81	15.33	14.95	16.04	15.12	17.83	14.86	16.13	15.29	18.22	23.33	15.01	15.81	20.85
Fe_2O_3	2.93	2.43	2.41	2.93	3.12	2.55	2.97	3.72	3.90	2.67	1.57	1.17	2.82	4.54	1.58
FeO	6.10	5.88	7.50	7.05	7.10	7.38	5.22	7.50	7.10	5.90	5.40	3.65	7.22	7.40	5.28
MnO	0.16	0.13	0.19	0.21	0.15	0.20	0.11	0.17	0.19	0.14	0.12	0.07	0.15	0.18	0.12
MgO	5.05	6.18	7.58	7.19	4.30	7.58	4.99	5.91	5.31	7.96	7.82	4.71	6.60	6.59	5.42
CaO	9.79	10.68	10.23	10.19	7.51	11.64	8.88	10.38	8.53	10.90	12.24	13.40	9.77	9.50	12.24
Na_2O	3.72	2.78	3.26	3.52	4.53	2.47	3.30	3.03	3.21	3.17	2.28	2.24	3.24	2.41	2.75
K_2O	1.02	1.30	0.58	0.71	0.94	0.58	2.05	1.00	1.56	0.44	0.30	0.56	1.35	0.95	0.30
P_2O_5	0.11	0.07	0.06	0.11	0.15	0.08	0.12	0.16	0.10	0.08	0.08	0.05	0.09	0.18	0.06
CO_2	0.04	0.09	0.09	0.04	0.07	0.07	0.07	0.11	0.17	0.22	0.17	0.02	0.02	0.02	0.07
H_2O	1.66	2.40	1.49	1.52	1.81	1.84	2.87	2.28	2.17	2.22	2.15	1.86	2.80	2.28	1.75
Total	99.83	99.84	99.82	99.80	99.83	99.82	99.80	99.81	99.79	99.82	99.83	99.83	99.82	99.79	99.82
$Mg^{\#}$	0.51	0.58	0.58	0.57	0.44	0.58	0.53	0.49	0.47	0.63	0.67	0.64	0.55	0.51	0.59
Sc	28.0	29.1	37.7	36.1	13.7	32.5	24.0	7.62	28.5	37.6	26.4	16.2	34.9	25.3	23.2
V	196	187	242	242	195	192	194	85.3	299	222	174	105	247	207	141
Cr	98.0	251	254	101	3.08	205	99.1	25.9	44.6	270	264	212	102	79.1	206
Co	24.8	31.6	36.9	35.5	25.5	30.7	23.5	11.5	30.4	33.0	33.8	20.8	36.3	33.2	27.7
Ni	35.4	57.2	44.5	47.6	12.4	53.5	50.7	15.5	32.3	62.3	107	53.7	45.4	60.7	54.6
Cu	16.2	18.0	43.5	39.9	14.4	10.2	5.00	51.0	9.38	67.5	6.71	4.90	53.2	28.5	44.5
Ga	18.6	15.8	16.5	16.5	20.8	14.1	18.4	17.5	18.6	15.2	15.4	15.2	16.2	20.1	15.8
Ge	1.62	1.55	1.55	1.65	1.55	1.48	1.61	0.950	1.66	1.53	1.38	1.11	1.66	1.55	1.23
Rb	33.8	63.0	12.4	25.8	35.5	15.3	96.5	37.1	72.6	9.62	6.63	11.9	31.1	24.5	5.15
Sr	302	294	262	279	299	255	403	770	365	270	274	424	262	429	385
Y	30.8	21.7	25.3	25.5	35.6	18.7	29.1	7.75	28.0	20.2	17.6	8.93	19.2	17.4	11.8
Zr	156	80.1	107	106	268	95.3	156	92.8	146	91.2	96.4	51.4	108	130	69.5
Nb	9.25	4.41	4.98	7.58	17.8	4.39	11.5	5.12	10.7	5.48	7.16	2.61	10.3	16.6	4.22
Cs	4.65	5.14	2.05	5.16	3.02	3.69	5.66	1.71	5.92	2.82	2.21	0.472	0.239	0.881	0.226
Ba	242	220	138	239	192	96.3	322	1000	354	134	79.9	97.2	171	270	83.6
La	8.84	5.32	5.78	7.11	11.6	3.95	10.7	20.6	8.76	4.39	5.29	2.83	5.46	10.4	4.31
Ce	20.0	13.7	16.4	18.7	28.7	11.7	25.4	40.5	21.9	11.6	13.1	6.91	13.5	24.3	10.5
Pr	2.86	2.10	2.57	2.83	4.25	1.88	3.54	4.86	3.36	1.86	1.98	1.06	1.98	3.27	1.53
Nd	13.6	10.3	12.5	13.4	19.3	9.21	16.2	18.6	15.1	8.94	9.25	4.73	9.34	14.4	7.19
Sm	4.22	3.05	3.63	3.77	5.21	2.64	4.26	3.28	4.13	2.66	2.58	1.33	2.76	3.69	1.86
Eu	1.36	1.11	1.31	1.28	1.65	1.02	1.87	1.07	1.48	1.04	1.01	0.633	1.20	1.38	0.838
Gd	5.33	3.66	4.47	4.50	5.91	3.18	5.12	2.60	5.01	3.28	3.09	1.47	3.29	3.85	2.26
Tb	1.01	0.689	0.811	0.851	1.12	0.587	0.949	0.337	0.916	0.669	0.574	0.282	0.631	0.663	0.386
Dy	6.32	4.26	5.06	5.27	7.08	3.78	5.91	1.74	5.70	4.02	3.51	1.79	3.92	3.88	2.44
Ho	1.33	0.882	1.08	1.08	1.51	0.779	1.22	0.310	1.19	0.870	0.732	0.379	0.794	0.740	0.503
Er	3.53	2.38	2.85	2.88	4.16	2.04	3.25	0.834	3.16	2.26	1.92	1.04	2.17	1.86	1.28
Tm	0.546	0.358	0.438	0.446	0.679	0.308	0.517	0.115	0.497	0.361	0.307	0.157	0.324	0.267	0.201
Yb	3.49	2.31	2.87	2.89	4.35	2.07	3.33	0.782	3.15	2.31	1.99	1.06	2.20	1.73	1.30
Lu	0.545	0.370	0.476	0.457	0.682	0.333	0.530	0.119	0.492	0.362	0.334	0.182	0.356	0.271	0.209
Hf	3.89	2.10	2.75	2.81	6.33	2.11	3.98	2.50	3.50	2.43	2.36	1.24	2.66	3.10	1.69
Ta	0.684	0.344	0.381	0.547	1.33	0.331	0.851	0.352	0.765	0.416	0.504	0.191	0.705	1.21	0.302
Pb	5.92	3.59	3.61	8.81	3.14	1.65	4.92	11.1	6.19	3.54	2.03	0.120	0.710	0.687	0.849
Th	1.65	0.687	0.471	0.730	2.91	0.427	1.36	2.83	1.04	0.496	0.683	0.279	0.742	1.41	0.565
U	0.492	0.228	0.209	0.309	0.976	0.123	0.768	0.938	0.337	0.149	0.191	0.0900	0.248	0.451	0.176

procedures are similar to those described by Li et al. (2006). Analytical precisions for most elements are better than 3%.

Sr and Nd isotopic analyses were performed on a Micromass Isoprobe multi-collector ICPMS at GIG-CAS, using analytical procedures described by Li et al. (2006). Sr and REE were separated using cation columns, and Nd fractions were further separated with HDEHP-coated Kef columns. Measured $^{87}Sr/^{86}Sr$ and $^{143}Nd/^{144}Nd$ ratios were normalized to $^{86}Sr/^{88}Sr = 0.1194$ and $^{146}Nd/^{144}Nd = 0.7219$, respectively. The reported $^{87}Sr/^{86}Sr$ and $^{143}Nd/^{144}Nd$ ratios were adjusted to the NBS SRM 987 standard $^{87}Sr/^{86}Sr = 0.71025$ and the Shin Etsu JNdi-1 standard $^{143}Nd/^{144}Nd = 0.512115$.

Argon isotope analyses were conducted on a MM-1200 mass spectrometer at the Analytical Center of Guilin Resource and Geological Institute following procedures similar to those described in Wang et al. (2007). The selected plagioclase grains from one Luotuogou gabbro sample were wrapped in Sn foil and sealed in 6 mm-ID evacuated quartz-glass vials together with ZBH-25 (biotite, 132.5 Ma) flux monitors, and irradiated for 37 h at the Beijing Nuclear Research Center. The monitor samples were individually fused and analyzed for argon isotope compositions. The plagioclases were step-heated using a radiofrequency furnace. All errors are quoted at the 1σ level and do not include the uncertainty of the monitor age.

4. Results

4.1. $^{40}Ar/^{39}Ar$ age of plagioclase

The $^{40}Ar/^{39}Ar$ dating results for plagioclase grains are shown in Table 1 and are further illustrated in Fig. 3. Eight steps between 480 °C and 1250 °C with 97.7% of ^{39}Ar release yielded a well-defined plateau age of 312 ± 1 Ma (MSWD = 1.2), which is consistent with the isochron age of 309 ± 6 Ma. The plagioclase $^{40}Ar/^{39}Ar$ dating sample (WXT789) is a fine-grained gabbro from the chilled margin of the intrusion. Thus, the plateau age is interpreted as the age of plagioclase crystallization. Our results are consistent with the three-sample whole-rock Rb–Sr isochron age of 321 ± 10 Ma reported by Zhu et al. (2006) for the Luotuogou gabbros, confirming that the gabbros formed in the Late Carboniferous.

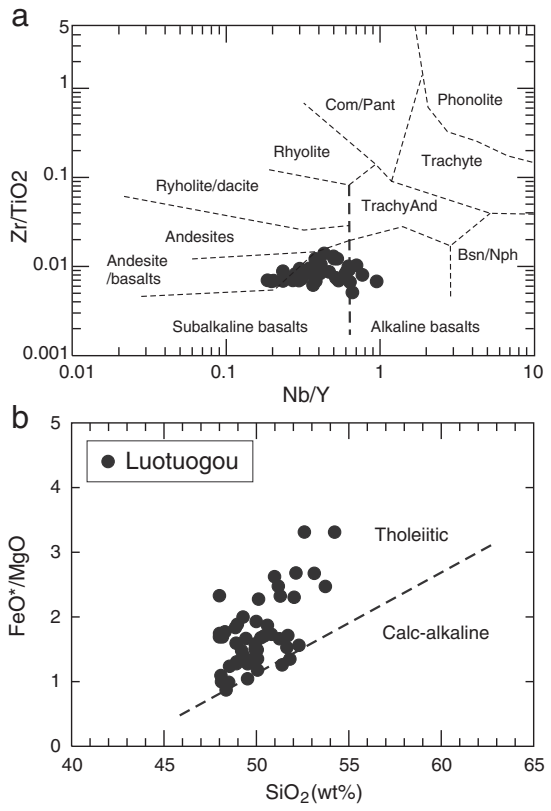

Fig. 6. (a) Nb/Y versus $Zr/TiO_2 \times 0.0001$ diagram distinguishing subalkaline and alkaline basalts (Winchester and Floys, 1977). (b) FeO*/MgO versus SiO_2 diagram distinguishing tholeiitic and calc-alkaline magma series (Miyashiro, 1974).

4.2. Mineral composition

Clinopyroxene in the gabbro mainly consists of augite and diopside, with a composition of $Wo_{38.5–47.4}$ $En_{31.9–48.4}$ $Fs_{7.3–22.9}$ (Appendix 1). Clinopyroxene chemical compositions display moderate variation (Mg-number = 59–87; SiO_2 = 48.66–52.59 wt.%; Al_2O_3 = 1.51–4.65 wt.%; TiO_2 = 0.42–1.92 wt.%; Cr_2O_3 = 0–11.37 wt.%; Na_2O = 0.30–20.61 wt.%). Clinopyroxene grains have cores of high $Mg^{\#}$, high Cr and low Ti and Na contents, and rims of relatively low $Mg^{\#}$ and Cr, and higher Ti and Na (Fig. 4).

Clinopyroxene grains are characterized by depletions in light rare earth elements (REEs) with $(La/Sm)_N$ = 0.16–0.42 and $(La/Yb)_N$ = 0.17–0.52, gently fractioned heavy REEs with $(Dy/Yb)_N$ = 1.1–1.6, and slightly negative Eu anomalies (Eu/Eu* ($=EuN/\sqrt[2]{SmN \times GdN}$)) (Appendix 2; Fig. 5a). Clinopyroxene rims have higher trace elements contents, and display slightly more pronounced negative Eu anomalies (Eu/Eu* = 0.65–0.93) than those of clinopyroxene cores (Eu/Eu* = 0.85–1.04), although they display similar REE patterns. On a primitive mantle-normalized diagram, they are characterized by negative anomalies in Nb, Zr and Ti, variable enrichments in Rb, Ba and Th, and, for the rims, strongly negative Sr anomalies (Fig. 5b).

4.3. Geochemical characteristics

Chemical compositions of the Luotuogou gabbros are listed in Table. 2. The gabbros have relatively high and variable SiO_2 (48.0–52.0 wt.%) and low MgO (6.2–7.4 wt.%) and TiO_2 (0.6–2.2 wt.%) contents. They are characterized by variable $Mg^{\#}$ ($100 \times Mg^{2+}/(Fe^{2+} + Mg^{2+})$) (35–67), Cr (3.08–578 ppm) and Ni (12.4–107 ppm) contents. These rocks have Nb/Y ratios of 0.19–0.96, plotting exclusively in the subalkaline-basalt field on the Nb/Y versus Zr/TiO_2 diagram of Winchester and Floyd (1976) (Fig. 6a). On the SiO_2 versus FeO^{Total}/MgO plot of Miyashiro (1974) (Fig. 6b), most samples exhibit typical tholeiite compositional trends with a wide range of FeO^{Total}/MgO, although a few samples plot in the calc-alkaline field.

On the chondrite-normalized REE plot, the Luotuogou gabbros are characterized by gently sloping REEs with normalized La/Yb of ~1.1–18.9, and slight positive Eu anomalies (Eu/Eu* = 0.77–1.37) (Fig. 7a). The rocks show "humped" REE patterns with variable enrichment in all incompatible elements such as Th and La, slightly negative or positive Nb and Ti anomalies (Fig. 7b). Their smooth REE and multi-trace element patterns are similar to that of enriched MORB (E-MORB). They have more variable and slightly higher Nb/La ratios (0.24–1.8, most > 0.7), and Zr (51.4–283 ppm) and Nb contents (4.2–24 ppm) relative to arc basalts, akin to Nb-enriched arc

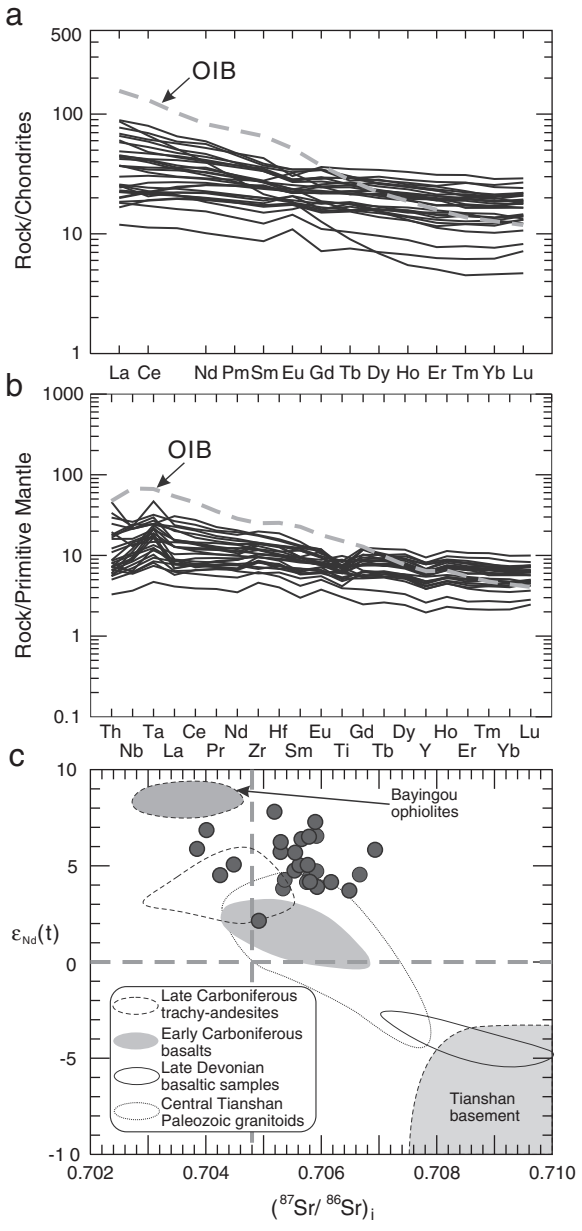

Fig. 7. Chondrite-normalized REE patterns and primitive mantle-normalized multi-element patterns of the Luotuogou gabbros (a–b). (c) Initial ε_{Nd} versus $^{87}Sr/^{86}Sr$ of the Luotuogou gabbros.
The composition of oceanic island basalts (OIB) and normalizing values are from Sun and McDonough (1989). Data for Bayingou ophiolites are from Xu et al. (2006); Data for Late Paleozoic volcanic rocks in the western Tianshan are from Zhu et al. (2009); The Central Tianshan Paleozoic granitoids are from Long et al. (2011); The Tianshan basement are from Hu et al. (2010).

Table 3
Sr–Nd isotopic composition of the Luotuogou gabbros.

Samples	Sm	Nd	$(^{143}Nd/^{144}Nd)_s$	2σ	$^{147}Sm/^{144}Nd$	$(^{143}Nd/^{144}Nd)_i$	$\varepsilon_{Nd}(t)$	Rb	Sr	$(^{87}Sr/^{86}Sr)_s$	2σ	$^{87}Rb/^{86}Sr$	$(^{87}Sr/^{86}Sr)_i$
wxt772	4.22	13.6	0.512866	0.000007	0.1891724	0.512482	4.7	33.8	301.6	0.706932	0.000016	0.316233	0.705537
wxt774	3.63	12.5	0.512891	0.000009	0.1770693	0.512532	5.7	12.4	261.7	0.705885	0.000011	0.133408	0.705297
wxt776	5.21	19.3	0.512899	0.000007	0.164138	0.512566	6.4	35.5	299.1	0.707134	0.000011	0.334622	0.705657
wxt782	4.13	15.1						72.6	364.8	0.708334	0.000011	0.560929	0.705860
wxt783	2.66	8.94	0.513006	0.000006	0.1809477	0.512639	7.8	9.62	269.9	0.705633	0.000013	0.100506	0.705190
wxt784	2.58	9.25	0.512934	0.000006	0.169561	0.512590	6.9	6.63	274	0.704313	0.000013	0.068197	0.704013
wxt785	1.33	4.73	0.512845	0.000012	0.1708232	0.512498	5.1	11.9	423.8	0.704832	0.000013	0.078854	0.704484
wxt787	3.69	14.4	0.512665	0.000006	0.1560275	0.512348	2.1	24.5	428.8	0.705629	0.000016	0.161196	0.704918
wxt789	1.86	7.19	0.512790	0.000007	0.1576582	0.512470	4.5	5.15	384.6	0.704415	0.000018	0.037741	0.704248

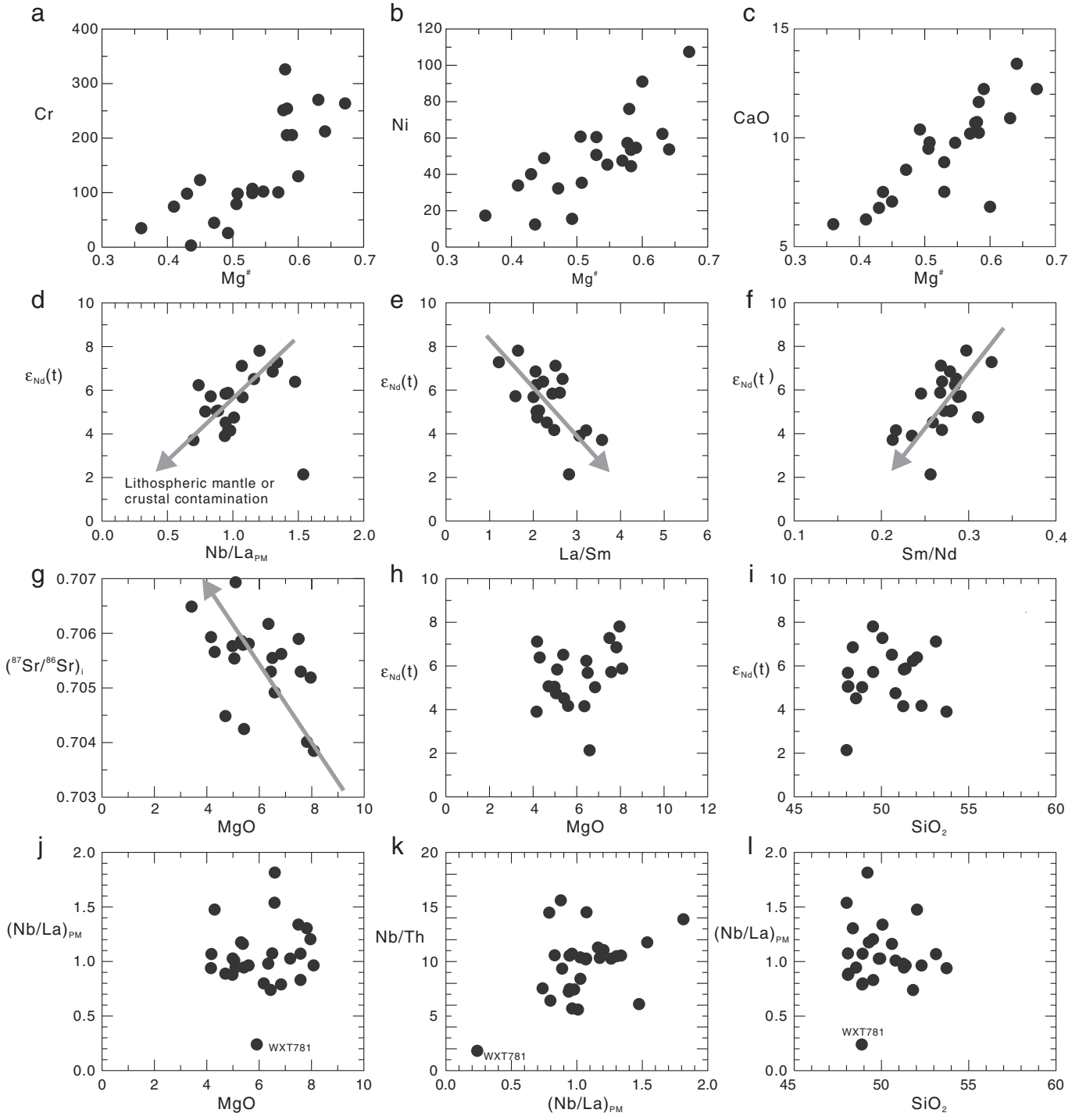

Fig. 8. Plots of isotope, element and elemental ratios of the Luotuogou gabbros.

basalts with high Na/La ratios (>0.5) or Nb contents (>7–16 ppm) (Sajona et al., 1996).

The Sr and Nd isotope compositions of the selected Luotuogou gabbros are presented in Table 3 and summarized in Fig. 7c. All initial isotopic ratios were corrected to 312 Ma using the plagioclase $^{40}Ar/^{39}Ar$ age obtained in this study. The samples have a wide range of initial $^{87}Sr/^{86}Sr$ values varying from 0.7039 to 0.7069, $^{147}Sm/^{144}Nd$ ratios between 0.1296 and 0.986, and initial $^{143}Nd/^{144}Nd$ ratios between 0.512429 and 0.512639, corresponding to initial $\varepsilon_{Nd}(t)$ values between +3.7 and +7.8. The only exception is sample WXT787 that has an $\varepsilon_{Nd}(t)$ value of +2.1. Such highly radiogenic Nd isotopic compositions suggest that the parental magmas of the Luotuogou gabbros were derived from a time-integrated depleted-mantle source.

5. Discussion

5.1. Fractional crystallization and crustal contamination

In general, mantle-derived primary melts have Ni>400 ppm and Cr>1000 ppm (Wilson, 1989), and $Mg^{\#}$ = 73–81 (Sharma, 1997). The Luotuogou samples exhibit variable MgO concentrations and $Mg^{\#}$ values, suggesting that they underwent fractional crystallization to varying degrees. They show large variations in $Mg^{\#}$ (35–67) and compatible elements such as Cr (3.08–578 ppm) and Ni (12.4–107 ppm). Their $Mg^{\#}$ contents are positively correlated with Cr and Ni contents (Fig. 8a–b), indicating a significant fractionation of olivine and chromite. In addition, there is a well-defined positive correlation between CaO and MgO (Fig. 8a–c), indicating a clinopyroxene-dominated fractionation.

When continental basaltic magmas rise from their sources in the mantle through the continental crust, they often experience contamination (Watson, 1982). One common way to assess the significance of crustal contamination is to assess correlations between indices of fractionation and the chemical and/or isotope data (Hawkesworth et al., 1995; Zhou et al., 2009). As shown in Fig. 8, the $\varepsilon_{Nd}(t)$ values of the Luotuogou gabbros are positively correlated with variable Nb/La_{PM} and Sm/Nd ratios and negatively correlated with variable La/Sm ratios (Fig. 8d–f). In addition, the MgO contents show a negative correlation with initial $^{87}Sr/^{86}Sr$ values (Fig. 8g). The observed variation correlations indicate that at least two isotopically distinct components were involved in the evolution of the Luotuogou samples. One component with relatively high ε_{Nd}, Nb/La, Sm/Nd and MgO, but low $^{87}Sr/^{86}Sr$ and La/Sm, is plausibly from the asthenospheric mantle. Another mixing component, characterized by low ε_{Nd}, Nb/La, Sm/Nd and MgO, but high $^{87}Sr/^{86}Sr$ and La/Sm, may have originated in the crust, the lithospheric mantle, or both (Xu et al., 2008).

Country rocks in the study area include Proterozoic granitic gneiss of the Tianshan basement rocks (Hu et al., 2000, 2010) and Central Tianshan Paleozoic granitoids (Long et al., 2011). As shown in Figs. 7c and 9, the Proterozoic granitic gneisses, characterized by a strongly negative $\varepsilon_{Nd}(t)$ or very low $(^{143}Nd/^{144}Nd)_i$ values, could not have been one of the contaminants, otherwise contamination would have resulted in low $\varepsilon_{Nd}(t)$ values for the Luotuogou gabbros. The Central Tianshan Paleozoic granitoids show slightly negative $\varepsilon_{Nd}(t)$ values and pronounced negative Nb anomalies (Nb/La as low as 0.3) and therefore are potential contaminants. Calculation suggests that up to 20% contamination of such crustal components is needed to account for the compositional variations observed in the Luotuogou gabbros (Fig. 9). However, such high degrees of felsic crust assimilation is untenable because it would have changed the bulk composition of the initial basaltic magma to an andesitic magma.

In addition, the absence of correlations of $\varepsilon_{Nd}(t)$ and Nb/La_{PM} with MgO and SiO_2, and of Nb/La with Nb/Th, are inconsistent with crustal contamination processes (Fig. 8h–l), given that continental crust is typically characterized by low $\varepsilon_{Nd}(t)$, MgO, and low Nb/La and Nb/Th ratios relative to that of the mantle (Rudnick and Fountain, 1995). Similarly,

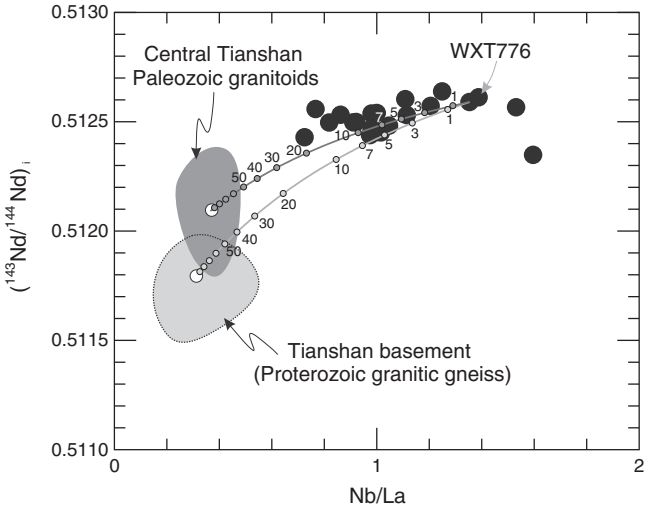

Fig. 9. Plot of $(^{143}Nd/^{144}Nd)_i$ vs. Nb/La for the Luotuogou gabbros showing the effects of crustal contamination. Numbers labeled on the binary mixing curve represent the percentages of crust components added to the melt. The contaminant crustal components of the Tianshan basement are the average of the Proterozoic gneiss (Nb = 14.2 ppm, La = 45.4 ppm, Nd = 41.0 ppm, and ε_{Nd}(312 Ma) = −8.7) (Hu et al., 2010), Paleozoic granitoid component of the Central Tianshan is from Long et al. (2011) (Nb = 13.1 ppm, La = 35.9 ppm, Nd = 32.6 ppm, and ε_{Nd}(312 Ma) = −2.9). The sample WXT776 is assumed to represents the primary magmas for Luotuogou gabbros (Nb = 17.8 ppm, La = 11.6 ppm, Nd = 19.3 ppm, and ε_{Nd}(312 Ma) = +6.4).

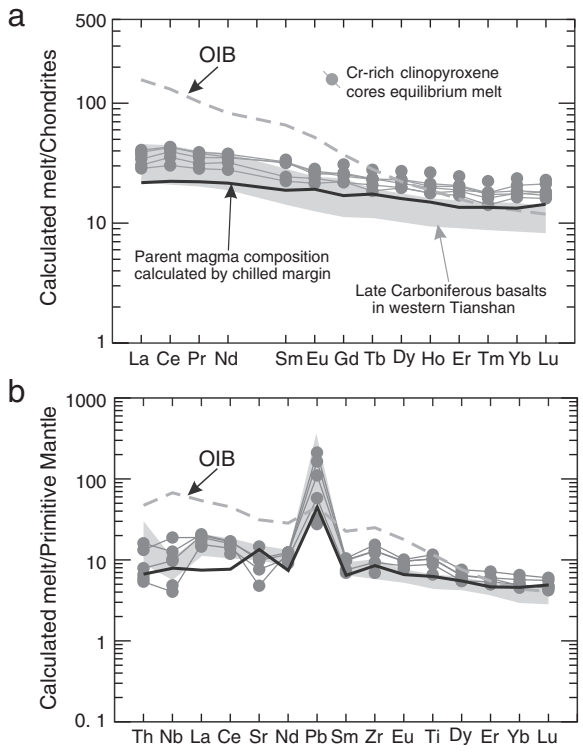

Fig. 10. Chondrite-normalized rare earth element (a) and primitive mantle normalized multi-element diagram (b) showing parent magma composition calculated by chilled margin, and the calculated melts for representative Cr-rich clinopyroxene cores in the Luotuogou gabbros.
Calculations were carried out using the clinopyroxene/basalt partition coefficients of Wood and Blundy (1997) and Hauri et al. (1994). The composition of oceanic island basalts (OIB) and the normalizing values are from Sun and McDonough (1989). The field of Late Carboniferous basalts in the western Tianshan is from Zhu et al. (2009) and Jiang et al. (2012).

both the cores and rims of the clinopyroxenes from the Luotuogou samples are characterized by strong depletions in LREEs (Fig. 5), which are also inconsistent with crustal contamination (Duggen et al., 2008). These lines of evidence therefore argue against crustal contamination as a controlling factor for the elemental and isotopic composition of the Luotuogou gabbros which must reflect characteristics of the mantle source.

5.2. Parental magma

The parental magma compositions of mafic intrusive rocks provide critical information for understanding their tectonic setting and mantle source characteristics (e.g., Wager and Brown, 1968). There are two common methods for establishing the parental magma compositions of mafic intrusions: a) analyzing the compositions of chilled margins or contemporaneous genetically related mafic sills and dikes (Greenwood et al., 1990; Hoover, 1989), and b) back-calculating the element abundances in parental melt in terms of cumulus-minerals element compositions and mineral/melt partition coefficients (Bernstein et al., 1996; Maier and Barnes, 1998).

We first estimated the parental magma compositions of the Luotuogou intrusive rocks by analyzing the compositions of the fine-grained gabbros identified at the contact zone between the intrusion and wall rocks. These chilled margins probably record the parental magma compositions of the Luotuogou intrusive rocks. This method, however, is only applicable if the chilled margins did not undergo crustal contamination or phenocryst accumulation. There is strong evidence arguing against crustal contamination for the Luotuogou gabbros as discussed above. The chilled margin of the Luotuogou intrusion is also nearly free of the phenocrysts. Consequently, the composition of the chilled margin appears to represent that of the parental magmas.

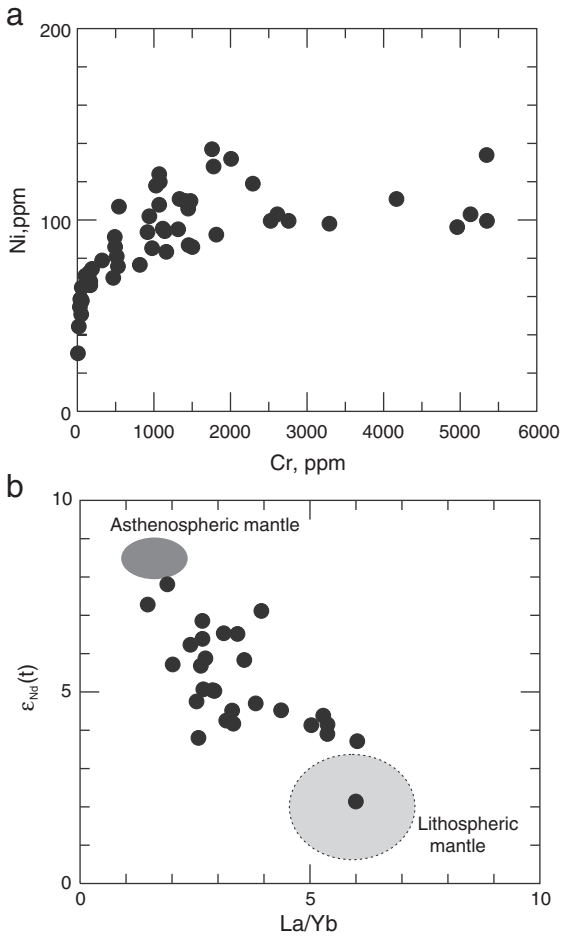

Fig. 11. (a) Clinopyroxene Cr and Ni concentrations. (b) Plot of $\varepsilon_{Nd}(t)$ vs. La/Yb for the Luotuogou gabbros.
The field of asthenospheric mantle represented by the Bayingou ophiolites in the western Tianshan is from Xu et al. (2006). The field of lithospheric mantle represented by western Tianshan Late Carboniferous arc basalts is from Zhou et al. (2009).

According to the above estimation, the parental magma of the Luotuogou intrusive rocks was a basaltic magma containing ~49.3 wt.% SiO_2 and ~7.1 wt.% MgO, enriched in FeO^T (~9.0 wt.%) and Al_2O_3 (~16.1 wt.%), indicating a ferrobasalt. Geochemically, they are comparable to the Late Carboniferous basalts in the western Tianshan (Jiang et al., 2012; Zhu et al., 2009). Geochemical modeling using the MELTS program (Ghiorso and Sack, 1995) indicates the magma could crystallize the most primitive mineral compositions (An_{72}) at a relatively high (~1212 °C) liquidus temperature and relatively low (FMQ: fayalite–magnetite–quartz) oxygen fugacity, which is consistent with those previously estimated for the Luotuogou gabbros (Zhu et al., 2006).

To further examine the reliability of the above estimated parental magma, we used the clinopyroxene/basalt partition coefficients of Hauri et al. (1994) and Wood and Blundy (1997) to calculate the Luotuogou melt compositions. The Cr-rich (>3000 ppm) clinopyroxene cores, which were probably sufficiently primitive to have crystallized before significant crystal fractionation, were selected to calculate melt compositions of the primary magmas of the Luotuogou gabbros (Dorais and Tubrett, 2008). The calculated La_N melt concentrations for the clinopyroxene Cr-rich cores range from 30 to 40 times chondrites with no negative Eu anomaly (Fig. 10a). The calculated melts are characterized by gently sloping REEs patterns, showing lower normalized concentration of LREEs and higher concentration of HREEs relative to that of the average gabbro composition (Fig. 10a). On a primitive mantle-normalized multi-elements plot (Fig. 10b), the calculated core liquids are rich in the highly incompatible elements, showing negligible to strongly negative Nb anomalies and pronounced positive Pb anomalies.

The Cr-rich pyroxene cores can be further assessed to establish whether or not their compositions correspond to those in equilibrium with primary magmas before the implications of the calculated results are discussed. The Mg number of the modeled liquids from which the Cr-rich cores crystallized ranges from 60 to 64, using the method of Wood and Blundy (1997), and the calculated liquids approach the primary basaltic magma compositions established in the Basaltic Volcanism Study Project (1981). There are no negative Eu anomalies on chondrite normalized REE plots and only minor Sr anomalies for a few samples on primitive mantle normalized multi-element plots (Fig. 10), indicating that no extensive plagioclase crystallization occurred (Dorais and Tubrett, 2008). On the plot of measured clinopyroxene Ni and Cr values (Fig. 11a), the most Cr-rich (>3000 ppm) clinopyroxene cores have low and constant Ni contents (~100 ppm) with declining Cr contents, indicating that significant fractional crystallization of olivine and chromite depleted the ambient liquid in Cr and Ni contents as clinopyroxene began to crystallize (Zhou et al., 1996). The olivine and chromite crystallization could have decreased the $Mg^{\#}$ (~60–64) of the residual liquids. However, olivine and chromite have distinctly low partition coefficients for the REEs and others incompatible elements (Dorais and Tubrett, 2008) listed in Fig. 10. Thus, the olivine and chromite crystallization could not have significantly changed the trace element patterns. Consequently, the trace element contents of calculated equilibrium melt using Cr-rich clinopyroxene cores should represent near-primary magma characteristics of the Luotuogou gabbros.

5.3. Nature of the mantle source characteristics

The most remarkable feature of the primary magmas that crystallized the Cr-rich cores is their enrichment in the large ion lithophile elements (LILEs), coupled with the negative to negligible Nb anomalies ($(Nb/La)_{PM} = 0.26–1.00$; $(Nb/Th)_{PM} = 0.74–1.74$) and strongly positive Pb anomalies. The whole rock compositions of the Luotuogou gabbros are characterized by large negative to positive Nb anomalies

$((Nb/La)_{PM} = 0.70–1.81$; $(Nb/Th)_{PM} = 0.47–1.86)$. However, as discussed above, crustal contamination did not play a major role in the formation of the Luotuogou gabbros. Therefore, the enrichment of the LILEs and negative Nb anomalies suggest a subduction zone component in the mantle source of the Luotuogou gabbros. The primary magmas are strongly enriched in Pb, and although the clinopyroxenes show a wide range of Ba/La values, their Th/Yb ratios have a smaller range (Appendix 2). These parameters suggest the input of subducted slab-derived fluids in the source of the parental magmas (Woodhead et al., 2001). The solubility of Pb and Ba in fluids is greater than that of Th, producing a range in Ba/La values for magmas derived from mantle sources influenced by subduction zone fluids. In contrast, a sedimentary input would produce a strong variation in Th/Yb values (Woodhead et al., 2001). The Luotuogou gabbros exhibit depleted mantle isotope character ($\varepsilon_{Nd}(t) = +3.7–+7.8$), and are geochemically similar to E-MORB, suggesting a MORB-type asthenosphere was involved in the Luotuogou magmas. The presence of residual hydrous mineral phases (e.g., amphibole), however, indicates that the Luotuogou magmas are in part derived from the lithospheric mantle. This is because these minerals are not stable in the hot and anhydrous convecting asthenosphere, but are stable under the conditions found in the lithospheric mantle (Class and Goldstein, 1997; Foley, 1992). Therefore, the Luotuogou samples likely represent melts derived from the asthenosphere mixed with melts from an enriched lithospheric mantle metasomatized by subducted slab-derived fluids.

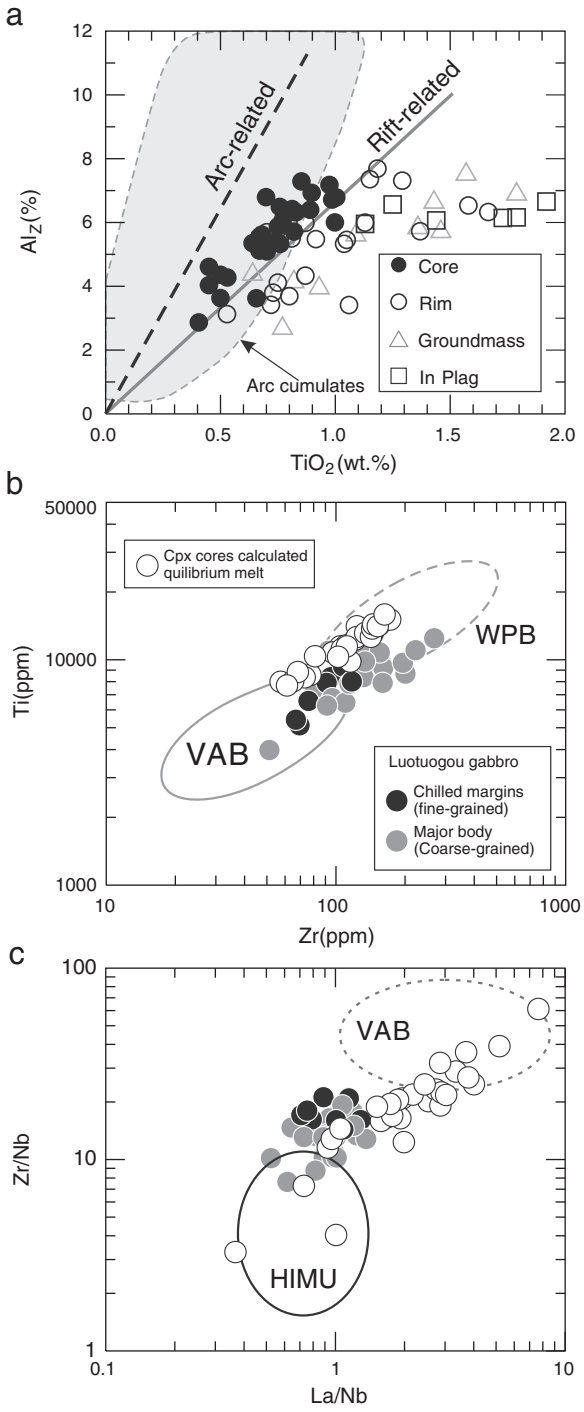

Fig. 12. (a) Plot of Al_Z (percentage of tetrahedral sites occupied by Al) vs. TiO_2 in clinopyroxenes. The reference trends of clinopyroxenes in rift and are-related mafic–ultramafic cumulates are from Loucks (1990), the arc cumulate area is after Zhou et al. (2007). Geochemical discrimination diagrams of (b) Ti–Zr (Pearce, 1996) and (c) Zr/Nb–La/Nb (Macera et al., 2008) for the Luotuogou gabbros.

The lithospheric mantle and asthenospheric mantle have different rheologies and distinct evolutionary histories. The lithospheric mantle generally remains an independent geochemical feature over geological time because it does not take part in mantle convection (Wilson et al., 1995). Thus, the lithospheric mantle can record distinct geochemical heterogeneities generated by subduction, generally showing enriched geochemical features. On the other hand, the asthenospheric mantle usually exhibits primitive or depleted geochemical features during moderate to large degrees of melting. In the present study, the regional asthenospheric mantle can best be represented by the northern Tianshan Early Carboniferous Bayingou ophiolites (344 Ma, with $\varepsilon_{Nd}(t)$ values ranging from +8 to +9 (Xu et al., 2006)). Carboniferous arc basalts in the western Tianshan, showing enriched isotope characteristic ($\varepsilon_{Nd}(t) < +2.0$), were considered to have been derived from the lithospheric mantle (Zhu et al., 2009). On the $\varepsilon_{Nd}(t)$–La/Y diagram (Fig. 11b), the Luotuogou gabbros show a clear transition trend from a metasomatized lithospheric mantle to an asthenospheric mantle.

Geochemical discrimination diagrams also suggest that the Luotuogou samples have dual, or hybrid, characteristics of both asthenospheric and metasomatized lithospheric mantle. The clinopyroxene compositions provide a further means for recognizing the tectonomagmatic affiliation of the gabbros. As a consequence of typically low H_2O and oxygen fugacities relative to arc-axis magmas, basaltic magmas in anorogenic igneous provinces, such as hotspot settings, are characterized by clinopyroxenes with lower Al_Z/TiO_2 (Al_Z = percentage of tetrahedral sites occupied by Al) (Loucks, 1990). Therefore, on a diagram of Al_Z versus TiO_2 in clinopyroxene (Fig. 12a), subduction-related clinopyroxenes yield an Al_Z/TiO_2 trend that is roughly twice as steep as that defined by clinopyroxenes from rift settings. Some of the Luotuogou samples plot along the rift-related cumulate trend and the others plot between the arc- and rift-related cumulates (Fig. 12a). On Zr–Ti and La/Nb–Zr/Nb plots (Fig. 12b–c), most samples fall in the transitional zone between the island arc basalt and within-plate basalt fields. The island arc characteristics of the Luotuogou gabbros indicate that a metasomatized lithospheric mantle component was involved in the source. In contrast, the presence of asthenospheric mantle generated the within-plate basalt compositional features of the Luotuogou gabbros.

5.4. Shallow melting depth

REE fractionation patterns can reflect the nature of the mantle source and the extent of melting (George et al., 2003). Despite the uncertainties related to the possible accumulation of pyroxene and the choice of clinopyroxene–melt partition coefficients, we conclude that the REE patterns of equilibrium melts (Figs. 10 and 13) should represent their parental melts as discussed in Section 5.2. Thus, the REE ratios of calculated melts should reflect the nature of the source and formation depth of the Luotuogou gabbros. The Luotuogou gabbros and calculated melts based on representative Cr-rich clinopyroxene cores all show weakly fractionated chondrite-normalized REE patterns, suggesting that their

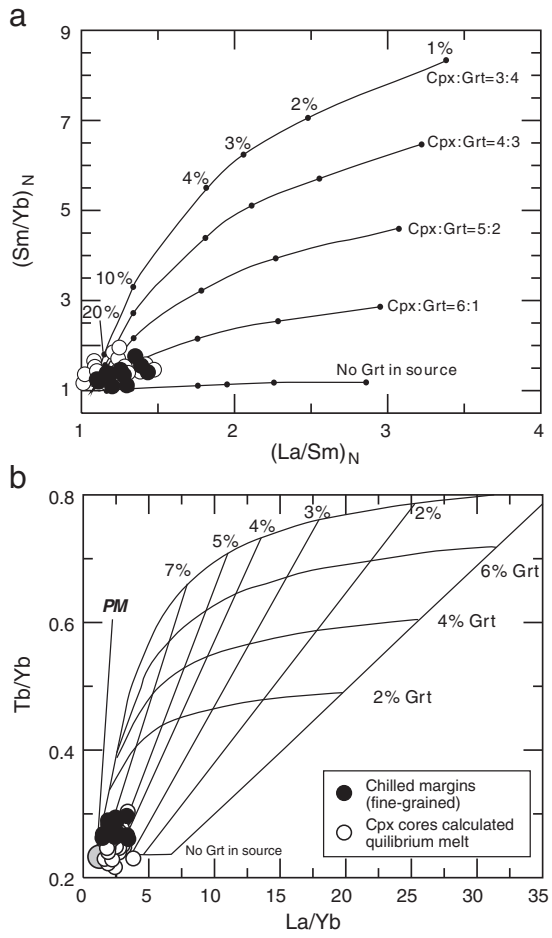

Fig. 13. (a) Sm/Yb versus La/Sm (D'Orazio et al., 2001) and Tb/Yb vs. La/Yb (George and Rogers, 2002) diagrams for the Luotuogou gabbros.

residue was garnet-poor. Fig. 13a shows $[Sm/Yb]_N$ versus $[La/Sm]_N$ for the Luotuogou gabbros, together with the batch equilibrium melting trends for various proportions of clinopyroxene and garnet left in the solid residue, for different degrees of partial melting (D'Orazio et al., 2001). Because Yb is compatible in garnet, whereas La and Sm are incompatible, La/Sm and Sm/Yb will be strongly fractionated when the degree of melting is low. In contrast, La/Sm is only slightly fractionated and Sm/Yb is nearly unfractionated during melting in the spinel stability field. The Luotuogou gabbros plot along melting trends with little to no garnet (Cpx:Grt = 6:1) in their source, and with more than 4% degrees of batch melting. This result is further confirmed by the La/Yb vs. Tb/Yb plot (Fig. 13b), which indicates the presence of less than 1% residual garnet in the source region for the Luotuogou gabbros. Based on calculations of REE fractionation, the degree of partial melting was about 7% (Fig. 13). Therefore, the Luotuogou mafic rocks were generated at a relatively shallow depth, mostly within the spinel stability field. If the depth of the spinel to garnet transition at the peridotite solidus occurs at ~75–80 km (McKenzie and O'Nions, 1991), then the result indicates that the decompressing asthenosphere rose to a relatively shallow level (<80 km).

The Luotuogou gabbros were most likely formed by the interaction between asthenospheric and metasomatized lithospheric mantle as discussed above. Further consideration is therefore required to assess whether the composition of asthenospheric melts contaminated by metasomatized lithospheric mantle can be used to infer the depth of melting. The lithosphere mantle-derived melts have distinctly higher La/Yb ratios than those of asthenospheric melts (Fig. 11b). Thus, the contamination of asthenospheric melts by lithosphere mantle-derived melts would increase La/Yb ratios, which would overestimate the melting depth for the source of the Luotuogou mafic rocks. Accordingly, the contamination process does not affect our inference that the magmas were derived from a shallow mantle source.

5.5. Geodynamic significance

McKenzie and Bickle (1988) proposed that dry asthenosphere can only melt once the lithosphere is thinned to <70–80 km. At least three competing mechanisms can be envisaged to account for the fact that Tianshan lithosphere was locally thinned to the extent that decompression melting of the asthenospheric mantle could occur: (1) mantle plume ascent; (2) slab break-off in a post-collisional setting; (3) slab roll-back.

Xia et al. (2004a, 2008) suggested that Carboniferous magmatic rocks in Tianshan Orogen represent a large igneous province related to a mantle plume. In particular, Xia et al. (2008) suggested that the Luotuogou mafic rocks occurred in a rift-related setting and were generated by higher degree (10–30%) partial melting of an asthenospheric OIB-like mantle source in the garnet stability field, probably originating from the plume center. However, our study indicates that the Luotuogou gabbros are dissimilar to OIB (Figs. 7a–b and 10) and were probably generated by mixing between asthenospheric and enriched lithospheric mantle melts at a relatively shallow depth, mostly within the spinel stability field. This suggests that they have an upper mantle source, which does not support the plume model proposed by Xia et al. (2004a, 2008).

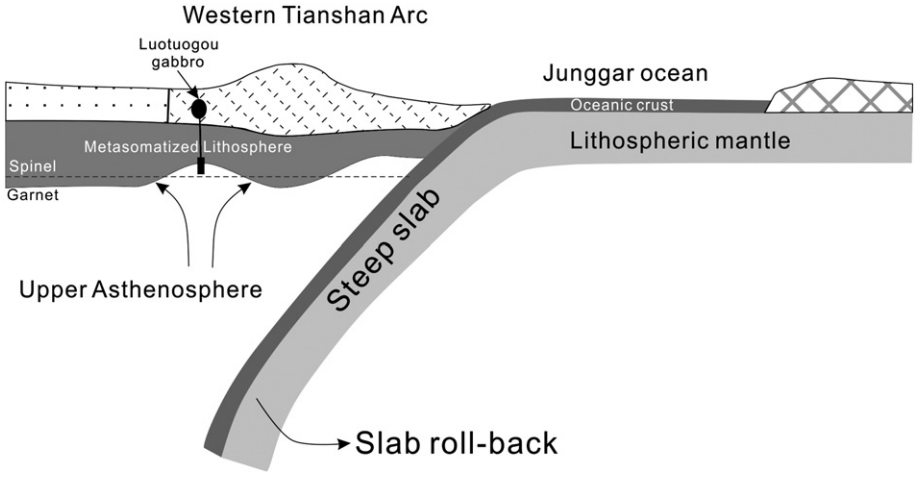

Fig. 14. Schematic presentations of a slab roll-back model to explain the generation of Luotuogou grabbro from Baluntai, Central Tianshan.

An olivine addition calculation can be used to extrapolate back to the composition of the parental magma and minimizes the effects of fractionation (Wang et al., 2002). The most primitive sample WXT783 (MgO = 7.96 wt.%; FeOt = 8.30 wt.%) has been modeled. Equilibrium olivine is added in 1% increments until the resulting basaltic magma is in equilibrium with Fo89 olivine and an $Mg^{\#}$ of 0.70 is attained (Fram and Lesher, 1997), using Kd = 0.31, where Kd is the molar ratio of FeO/MgO in olivine to that in the coexisting magma (Roeder and Emslie, 1970), and assuming Fe^{2+}/total Fe = 0.85. After removing the effect of 11% olivine crystallization, the primary magma contains MgO = 11.84 wt.%, and FeOt = 8.71 wt.%. The MgO content of the resulting primary magma is lower than that of the mantle plume derived basalts (Sharma, 1997), which further supports our results from REE modeling and other approaches.

In addition to gabbros, Carboniferous adakites also occur in the Luotuogou area and are characterized by positive $\varepsilon_{Nd}(t)$ values (+1.8–+8.5), low initial $^{87}Sr/^{86}Sr$ ratios (0.7026–0.7051) and high $Mg^{\#}$ (>40). These adakites are considered to have been generated by partial melting of subducted Junggar Oceanic crust (Wang et al., 2006; Xiong et al., 2005), which is also difficult to reconcile with a mantle plume model. Other geological and geochemical evidence also argues against a mantle plume model for the Tianshan Carboniferous magmas (Tang et al., 2010; Wang et al., 2007; Zhu et al., 2005, 2009). For example, widely distributed Carboniferous volcanic rocks in the Tianshan consist mainly of calc-alkaline intermediate-felsic volcanic rocks, with less significant amounts of mafic rocks (Zhu et al., 2005). All these rocks show typical island arc-type geochemical features: enrichment in LILEs and depletion in high field strength elements (Tang et al., 2010; Wang et al., 2007; Zhu et al., 2005, 2009). Thus, a diverse range of evidence indicates that the formation of the Luotuogou gabbros was not related to a Carboniferous mantle plume.

Recently, Yuan et al. (2010) proposed that Late Carboniferous (301 ± 6 Ma) gabbro in the eastern Tianshan was formed in a slab break-off regime after the closure of the Kelameili Ocean. Based on the study of ~316 Ma Sikeshu pluton granites near the Bayingou ophiolite in the Northern Tianshan Terrane, Han et al. (2010) also suggested a slab break-off and asthenosphere upwelling model after the collision between the Junggar Plate and the Kazakhstan–Yili Block. However, we suggest for several reasons that the Luotuogou mafic magmas could not have been related to a slab break-off environment. In the western part of the Tianshan, widely distributed Late Carboniferous arc-type magmas, e.g., the Dahalajunshan Formation trachy–andesites–rhyolites from the western Tianshan, formed between 324 and 312 Ma, and are characterized by high $\varepsilon_{Nd}(t)$ values (+2.79–+5.89) and low initial $^{87}Sr/^{86}Sr$ ratios (0.7032–0.7054), and positive zircons $\varepsilon_{Hf}(t)$ values with weighted average values of +10.3, indicating basaltic rocks among them were derived by partial melting of the mantle wedge (Zhu et al., 2005, 2009); Quartz diorites and dacites from the North Tianshan Terrane formed between 316 and 309 Ma, with positive $\varepsilon_{Nd}(t)$ values (+0.1–+3.3), generated by melting of juvenile basaltic arc lower crust (Niu et al., 2010; Tang et al., 2010). All of these rocks have the geochemical characteristics of arc volcanic rocks (e.g., enrichment of LILEs and strong negative anomalies of Ta, Nb, and Ti), and most probably formed at an active continental arc setting due to the southward subduction of the North Tianshan Oceanic Plate beneath the Kazakhstan–Yili Block. Recent studies of Early Permian mafic–ultramafic complexes from the Beishan area in the southernmost CAOB suggest they were emplaced in the subduction-related environment (Ao et al., 2010). They also indicate that particular examples of accretionary orogenesis in the southern part of the CAOB may represent episodes within a longer-lived process (Ao et al., 2010; Xiao et al., 2009). Consequently, multiple episodes of accretion likely occurred in the CAOB (Xiao et al., in press) and were likely to be still ongoing during the Late Carboniferous in the western Tianshan.

There is a magmatic gap or quiescent period in the Northern Tianshan Terrane between ca. 345 and 320 Ma that has been attributed to a period of "flat-subduction" (Fig. 13b of Tang et al., 2010). However, the appearance of the Late Carboniferous magmatism indicates that the continental arc setting persisted until ca. 312 Ma in western Tianshan. Such a transition from flat- to normal angle subduction suggests that the oceanic slab likely underwent a roll-back stage to return to a normal-angle subduction (Fig. 14). An analogous transition process has been documented along the entire Andean system, and it has experienced flat and normal-angle subduction processes (Kay and Mpodozis, 2001; Ramos and Folguera 2009). During the transition process from flat- to normal angle subduction, upwelling asthenospheric mantle would have led to decompressional melting and would also have provided the heat source for the partial melting of overlying lithospheric mantle that had previously been metasomatized by subduction. Accordingly, the Luotuogou gabbros were most probably generated by mixing between the upwelling asthenospheric mantle-derived and metasomatized lithospheric mantle-derived melts at a shallower level.

6. Conclusions

New plagioclase $^{40}Ar/^{39}Ar$ dating provides a Late Carboniferous (312 ± 1 Ma) emplacement age for the Luotuogou gabbros in the Central Tianshan Terrane of the Tianshan Orogen. The gabbros exhibit typical tholeiite compositional trends with depleted isotope compositions ($\varepsilon_{Nd}(t)$ = +3.7–+7.8). They have dual, or hybrid, geochemical characteristics of within-plate and island arc magmatism. The primary magmas calculated from clinopyroxene Cr-rich cores are enriched in the LILEs, coupled with negative Nb anomalies and strongly positive Pb anomalies, indicating a subduction zone component in the mantle source of the Luotuogou gabbros. They were likely produced by the mixing between asthenospheric mantle-derived and enriched lithospheric mantle-derived melts. The formation of the Luotuogou gabbros was not related to mantle plume ascent, but to slab roll-back.

Supplementary data to this article can be found online at http://dx.doi.org/10.1016/j.lithos.2012.08.015.

Acknowledgments

We are grateful to Professors Nelson Eby and Wenjiao Xiao and an anonymous reviewer for their critically constructive reviews, which allowed us to improve the present discussion greatly. We appreciate the assistance of Wei-Dong Sun, Tong-Mo Dai, Ying Liu, Guang-Qian Hu, Xi-Rong Liang, Xiang-Lin Tu and Hong Zhang for geochemical analyses. This study was jointly supported by the Major State Basic Research Program (973 Program) of the People's Republic of China (nos. 2011CB808906 and 2007CB411308), the National Natural Science Foundation of China (grants nos. 41025006, 41073029 and 41121002). This is contribution No. IS-1558 from GIGCAS, TIGeR (The Institute for Geoscience Research) publication # 429, and contribution 212 from the ARC Centre of Excellence for Core to Crust Fluid Systems (http://www.ccfs.mq.edu.au/).

References

Allen, M.B., Windley, B.F., Zhang, C., 1993. Palaeozoic collisional tectonics and magmatism of the Chinese Tien Shan, central Asia. Tectonophysics 220, 89–115.
Ao, S.J., Xiao, W.J., Han, C.M., Mao, Q.G., Zhang, J.E., 2010. Geochronology and geochemistry of Early Permian mafic–ultramafic complexes in the Beishan area, Xinjiang, NW China: implications for late Paleozoic tectonic evolution of the southern Altaids. Gondwana Research 18, 466–478.
Basaltic Volcanism Study Project, 1981. Basaltic Volcanism on the Terrestrial Planets. Pergamon, New York.
Bernstein, S., Kelemen, P.B., Brooks, C.K., 1996. Evolution of the Kap Edward Holm Complex: a mafic intrusion at a rifted continental margin. Journal of Petrology 37, 497–519.
Campbell, I.H., Griffiths, R.W., 1990. Implications of mantle plume structure for the evolution of flood basalts. Earth and Planetary Science Letters 99, 79–93.
Che, Z.L., Liu, L., 1996. Review on the ancient Yil i Rift, Xingjian, China. Acta Petrologica Sinica 12, 478–490 (in Chinese with English abstract).

Chen, B., Suzuki, K., Tian, W., Jahn, B., Ireland, T., 2009. Geochemistry and Os–Nd–Sr isotopes of the Gaositai Alaskan-type ultramafic complex from the northern North China craton: implications for mantle–crust interaction. Contributions to Mineralogy and Petrology 158, 683–702.
Class, C., Goldstein, S.L., 1997. Plume–lithosphere interactions in the ocean basins: constraints from the source mineralogy. Earth and Planetary Science Letters 150, 245–260.
Coney, P.J., Reynolds, S.J., 1977. Cordilleran Benioff zones. Nature 270, 403–406.
D'Orazio, M., Agostini, S., Innocenti, F., Haller, M.J., Manetti, P., Mazzarini, F., 2001. Slab window-related magmatism from southernmost South America: the Late Miocene mafic volcanics from the Estancia Glencross Area (52°S, Argentina–Chile). Lithos 57, 67–89.
Dong, Y., Zhang, G., Neubauer, F., Liu, X., Hauzenberger, C., Zhou, D., Li, W., 2011. Syn- and post-collisional granitoids in the Central Tianshan orogen: geochemistry, geochronology and implications for tectonic evolution. Gondwana Research 20, 568–581.
Dorais, M.J., Tubrett, M., 2008. Identification of a subduction zone component in the Higganum dike, Central Atlantic Magmatic Province: a LA–ICPMS study of clinopyroxene with implications for flood basalt petrogenesis. Geochemistry, Geophysics, Geosystems 9 http://dx.doi.org/10.1029/2008gc002079.
Duggen, S., Hoernle, K., Klügel, A., Geldmacher, J., Thirlwall, M., Hauff, F., Lowry, D., Oates, N., 2008. Geochemical zonation of the Miocene Alborán Basin volcanism (westernmost Mediterranean): geodynamic implications. Contributions to Mineralogy and Petrology 156, 577–593.
Fram, M.S., Lesher, C.E., 1997. Generation and polybaric differentiation of Greenland Early Tertiary flood basalts. Journal of Petrology 38, 231–275.
Foley, S., 1992. Vein-plus-wall-rock melting mechanisms in the lithosphere and the origin of potassic alkaline magmas. Lithos 28, 435–453.
Gao, J., Klemd, R., Qian, Q., Zhang, X., Li, J., Jiang, T., Yang, Y.Q., 2011. The collision between the Yili and Tarim blocks of the Southwestern Altaids: geochemical and age constraints of a leucogranite dike crosscutting the HP–LT metamorphic belt in the Chinese Tianshan Orogen. Tectonophysics 499, 118–131.
Gao, J., Li, M.S., Xiao, X.C., Tang, Y.Q., He, G.Q., 1998. Paleozoic tectonic evolution of the Tianshan Orogen, northwestern China. Tectonophysics 287, 213–231.
Gao, J., Long, L., Klemd, R., Qian, Q., Liu, D., Xiong, X., Su, W., Liu, W., Wang, Y., Yang, F., 2009. Tectonic evolution of the South Tianshan orogen and adjacent regions, NW China: geochemical and age constraints of granitoid rocks. International Journal of Earth Sciences 98, 1221–1238.
Garfunkel, Z., 2008. Formation of continental flood volcanism — the perspective of setting of melting. Lithos 100, 49–65.
George, R., Rogers, N., 2002. Plume dynamics beneath the African plate inferred from the geochemistry of the Tertiary basalts of southern Ethiopia. Contributions to Mineralogy and Petrology 144, 286–304.
George, R., Turner, S., Hawkesworth, C., Morris, J., Nye, C., Ryan, J., Zheng, S.H., 2003. Melting processes and fluid and sediment transport rates along the Alaska–Aleutian arc from an integrated U–Th–Ra–Be isotope study. Journal of Geophysical Research-Solid Earth 108 (B5), 2252 http://dx.doi.org/10.1029/2002JB001916.
Greenwood, R.C., Donaldson, C.H., Emeleus, C.H., 1990. The contact zone of the Rhum ultrabasic intrusion: evidence of peridotite formation from magnesian magmas. Royal Society of London Geophysical Journal 147, 209–212.
Ghiorso, M.S., Sack, R.O., 1995. Chemical mass transfer in magmatic processes. IV. A revised and internally consistent thermodynamic model for the interpolation and extrapolation of liquid–solid equilibria in magmatic systems at elevated temperatures and pressures. Contributions to Mineralogy and Petrology 119, 197–212.
Han, B.F., Guo, Z.J., Zhang, Z.C., Zheng, L., Chen, J.F., Song, B., 2010. Age, geochemistry, and tectonic implications of a late Paleozoic stitching pluton in the North Tian Shan suture zone, western China. Geological Society of America Bulletin 122, 627–640.
Hao, J., Liu, X.H., 1993. Ophiolite melange time and tectonic evolutional model in South Tianshan area. Chinese Journal of Geology 28, 93–95.
Hauri, E.H., Wagner, T.P., Grove, T.L., 1994. Experimental and natural partitioning of Th, U, Pb and other trace elements between garnet, clinopyroxene and basaltic melts. Chemical Geology 117, 149–166.
Hawkesworth, C.J., Lightfoot, P.C., Fedorenko, V.A., Blake, S., Naldrett, A.J., Doherty, W., Gorbachev, N.S., 1995. Magma differentiation and mineralisation in the Siberian continental flood basalts. Lithos 34, 61–88.
Hoernle, K., White, J.D.L., van den Bogaard, P., Hauff, F., Coombs, D.S., Werner, R., Timm, C., Garbe-Schönberg, D., Reay, A., Cooper, A.F., 2006. Cenozoic intraplate volcanism on New Zealand: upwelling induced by lithospheric removal. Earth And Planetary Science Letters 248, 350–367.
Hoover, J.D., 1989. The chilled marginal gabbro and other contact rocks of the Skaergaard intrusion. Journal of Petrology 30, 441–476.
Hu, A.Q., Jahn, B.M., Zhang, G.X., Chen, Y.B., Zhang, Q.F., 2000. Crustal evolution and Phanerozoic crustal growth in northern Xinjiang: Nd isotopic evidence. Part I. Isotopic characterization of basement rocks. Tectonophysics 328, 15–51.
Hu, A.Q., Wei, G.J., Jahn, B.M., Zhang, J.B., Deng, W.F., Chen, L.L., 2010. Formation of the 0.9Ga Neoproterozoic granitoids in the Tianshan Orogen, NW China: constraints from the SHRIMP zircon age determination and its tectonic significance. Geochimica 39, 197–212 (In Chinese with English abstract).
Huang, X.L., Xu, Y.G., Lo, C.H., Wang, R.C., Lin, C.Y., 2007. Exsolution lamellae in a clinopyroxene megacryst aggregate from Cenozoic basalt, Leizhou Peninsula, South China: petrography and chemical evolution. Contributions to Mineralogy and Petrology 154, 691–705.
Jahn, B.M., Wu, F.Y., Chen, B., 2000. Massive granitoid generation in Central Asia: Nd isotope evidence and implication for continental growth in the Phanerozoic. Episodes 23, 82–92.
Jiang, Z.S., Zhang, Z.H., Hou, K.J., Hong, W., Wang, Z.H., Li, F.M., Tian, J.Q., 2012. Geochemistry and zircon U–Pb ages of volcanic rocks from the Chagangnuoer and Zhibo iron deposits, western Tianshan, and their geological significance. Acta Petrologica Sinica 28, 2074–2088.
Kay, S.M., Mpodozis, C., 2001. Central Andean ore deposits linked to evolving shallow subduction systems and thickening crust. GSA Today 11 (3), 4–9.
Li, X.H., Li, Z.X., Wingate, M.T.D., Chung, S.L., Liu, Y., Lin, G.C., Li, W.X., 2006. Geochemistry of the 755 Ma Mundine Well dyke swarm, northwestern Australia: part of a Neoproterozoic mantle superplume beneath Rodinia? Precambrian Research 146, 1–15.
Li, Z.X., Li, X.H., 2007. Formation of the 1300-km-wide intracontinental orogen and postorogenic magmatic province in Mesozoic South China: a flat-slab subduction model. Geology 35, 179–182.
Liu, Y.S., Hu, Z.C., Gao, S., Günther, D., Xu, J., Gao, C.G., Chen, H.H., 2008. In situ analysis of major and trace elements of anhydrous minerals by LA–ICP-MS without applying an internal standard. Chemical Geology 257, 34–43.
Long, L., Gao, J., Klemd, R., Beier, C., Qian, Q., Zhang, X., Wang, J., Jiang, T., 2011. Geochemical and geochronological studies of granitoid rocks from the Western Tianshan Orogen: implications for continental growth in the southwestern Central Asian Orogenic Belt. Lithos 126, 321–340.
Loucks, R.R., 1990. Discrimination of ophiolitic from nonophiolitic ultramafic–mafic allochthons in orogenic belts by the Al/Ti ratio in clinopyroxene. Geology 18, 346–349.
Macera, P., Gasperini, D., Ranalli, G., Mahatsente, R., 2008. Slab detachment and mantle plume upwelling in subduction zones: an example from the Italian South-Eastern Alps. Journal of Geodynamics 45, 32–48.
Maier, W., Barnes, S.-J., 1998. Rare earth elements in the Bushveld complex — a complete stratigraphic section. Chemical Geology 103, 85–103.
McKenzie, D., Bickle, M., 1988. The volume and composition of melt generated by extension of the lithosphere. Journal of Petrology 29, 625–679.
McKenzie, D., O'Nions, R.K., 1991. Partial melt distributions from inversion of rare earth element concentrations. Journal of Petrology 32, 1021–1091.
Miyashiro, A., 1974. Volcanic rock series in island arcs and active continental margins. American Journal of Science 274, 321–355.
Niu, H.C., Shan, Q., Luo, Y., Yang, W.B., Zhou, C.P., Liao, S.P., Xu, X.Y., 2010. Geochronological and geochemical studies on quartz diorite in Yuximolegai Daban. West Tianshan and its tectonic implication. Acta Petrologica Sinica 26, 2935–2945 (in Chinese with English abstract).
Pearce, J.A., 1996. A user's guide to basalt discrimination diagrams. In: Wyman, D.A. (Ed.), Trace Element Geochemistry of Volcanic Rocks: Applications for Massive Sulphide Exploration Geological Association of Canada, pp. 79–113.
Qian, Q., Gao, J., Klemd, R., He, G., Song, B., Liu, D., Xu, R., 2009. Early Paleozoic tectonic evolution of the Chinese South Tianshan Orogen: constraints from SHRIMP zircon U–Pb geochronology and geochemistry of basaltic and dioritic rocks from Xiate, NW China. International Journal of Earth Sciences 98, 551–569.
Ramos, V.A., Folguera, A., 2009. Andean flat-slab subduction through time. Geological Society, London, Special Publication 327 (1), 31–54.
Roeder, P.L., Emslie, R.F., 1970. Olivine–liquid equilibrium. Contributions to Mineralogy and Petrology 29, 275–289.
Rudnick, R.L., Fountain, D.M., 1995. Nature and composition of the continental crust: a lower crustal perspective. Reviews of Geophysics 33, 267–309.
Sajona, F.G., Maury, R.C., Bellon, H., Cotten, J., Defant, M., 1996. High field strength element enrichment of Pliocene–Pleistocene Island arc basalts, Zamboanga Peninsula, western Mindanao (Philippines). Journal of Petrology 37, 693–726.
Saunders, A.D., 2005. Large igneous provinces: origin and environmental consequences. Elements 1, 259–263.
Sengör, A.M.C., Natal'in, B.A., Burtman, V.S., 1993. Evolution of the Altaid tectonic collage and Palaeozoic crustal growth in Eurasia. Nature 364, 299–307.
Sharma, M., 1997. Siberian traps. In: Mahoney, J.J., Coffin, M.F. (Eds.), Large Igneous Provinces: Continental, Oceanic, and Planetary Flood Volcanism. American Geophysical Union, pp. 273–295.
Shi, Y., Liu, D., Zhang, Q., Jian, P., Zhang, F., Miao, L., 2007. SHRIMP zircon U–Pb dating of the Gangou granitoids, central Tianshan Mountains, northwest China and tectonic significances. Chinese Science Bulletin 52, 1507–1516.
Sun, S.S., McDonough, W.F., 1989. Chemical and isotopic systematics of oceanic basalts: implications for mantle composition and processes. In: Saunders, A.D., Norry, M.J. (Eds.), Magmatism in the Ocean Basins: Geological Society London Special Publications, pp. 313–345.
Tang, G.J., Wang, Q., Wyman, D.A., Sun, M., Li, Z.X., Zhao, Z.H., Sun, W.D., Jia, X.H., Jiang, Z.Q., 2010. Geochronology and geochemistry of Late Paleozoic magmatic rocks in the Lamasu–Dabate area, northwestern Tianshan (west China): evidence for a tectonic transition from arc to post-collisional setting. Lithos 119, 393–411.
Timm, C., Hoernle, K., Van Den Bogaard, P., Bindeman, I., Weaver, S., 2009. Geochemical evolution of intraplate volcanism at Banks Peninsula, New Zealand: interaction between asthenospheric and lithospheric melts. Journal of Petrology 50, 989–1023.
Tribuzio, R., Renna, M.R., Braga, R., Dallai, L., 2009. Petrogenesis of Early Permian olivine-bearing cumulates and associated basalt dykes from Bocca di Tenda (Northern Corsica): implications for post-collisional Variscan evolution. Chemical Geology 259, 190–203.
Tribuzio, R., Tiepolo, M., Fiameni, S., 2008. A mafic–ultramafic cumulate sequence derived from boninite-type melts (Niagara Icefalls, northern Victoria Land, Antarctica). Contributions to Mineralogy and Petrology 155, 619–633.
Wager, L., Brown, G., 1968. Layered Igneous Rocks. Oliver and Boyd, Edinburgh . 588.
Wang, K., Plank, T., Walker, J.D., Smith, E.I., 2002. A mantle melting profile across the Basin and Range, SW USA. Journal of Geophysical Research 107 (B1), 2017 http://dx.doi.org/10.1029/2001JB000209.
Wang, Q., Wyman, D.A., Zhao, Z.H., Xu, J.F., Bai, Z.H., Xiong, X.L., Dai, T.M., Li, C.F., Chu, Z.Y., 2007. Petrogenesis of Carboniferous adakites and Nb-enriched arc basalts in the Alataw area, northern Tianshan Range (western China): implications for Phanerozoic crustal growth in the Central Asia orogenic belt. Chemical Geology 236, 42–64.

Wang, Q., Zhao, Z.H., Xu, J.F., Wyman, D.A., Xiong, X.L., Zi, F., Bai, Z.H., 2006. Carboniferous adakite-high-Mg andesite-Nb-enriched basaltic rock suites in the Northern Tianshan area: implications for Phanerozoic crustal growth in the Central Asia Orogenic Belt and Cu–Au mineralization. Acta Petrologica Sinica 22 (1), 11–30 (in Chinese with English abstract).

Watson, E.B., 1982. Basalt contamination by continental crust: some experiments and models. Contributions to Mineralogy and Petrology 80, 73–87.

Wilson, M., 1989. Igneous Petrogenesis. Springer, Harper Collins Academic, London. p. 466.

Wilson, M., Rosenbaum, J.M., Dunworth, E.A., 1995. Melilitites: partial melts of the thermal boundary layer? Contributions to Mineralogy and Petrology 119, 181–196.

Winchester, J.A., Floyd, P.A., 1976. Geochemical magma type discrimination: application to altered and metamorphosed basic igneous rocks. Earth and Planetary Science Letters 28, 459–469.

Winchester, J.A., Floys, P.A., 1977. Geochemical discrimination of different magma series and their differentiation products using immobile elements. Chemical Geology 20, 325–343.

Windley, B.F., Alexeiev, D., Xiao, W., Kroner, A., Badarch, G., 2007. Tectonic models for accretion of the Central Asian Orogenic Belt. Journal of the Geological Society of London 164, 31–47.

Windley, B.F., Allen, M.B., Zhang, C., Zhao, Z.Y., Wang, G.R., 1990. Paleozoic accretion and Cenozoic redeformation of the Chinese Tien Shan Range, Central Asia. Geology 18, 128–131.

Wood, B.J., Blundy, J.D., 1997. A predictive model for rare earth element partitioning between clinopyroxene and anhydrous silicate melt. Contributions to Mineralogy and Petrology 129, 166–181.

Woodhead, J.D., Hergt, J.M., Davidson, J.P., Eggins, S.M., 2001. Hafnium isotope evidence for 'conservative' element mobility during subduction zone processes. Earth and Planetary Science Letters 192, 331–346.

Xia, L.Q., Xia, Z.C., Xu, X.Y., Li, X.M., Ma, Z.P., 2008. Relative contributions of crust and mantle to the generation of the Tianshan Carboniferous rift-related basic lavas, northwestern China. Journal of Asian Earth Sciences 31, 357–378.

Xia, L.Q., Xia, Z.C., Xu, X.Y., Li, X.M., Ma, Z.P., Wang, L.S., 2004a. Carboniferous Tianshan igneous megaprovince and mantle plume. Geologcal Bulletin of China 23, 903–910 (in Chinese with English abstract).

Xia, L.Q., Xu, X.Y., Xia, Z.C., Li, X.M., Ma, Z.P., Wang, L.S., 2004b. Petrogenesis of Carboniferous rift-related volcanic rocks in the Tianshan, northwestern China. Geological Society of America Bulletin 116, 419–433.

Xiao, W.J., Han, C.M., Yuan, C., Sun, M., Lin, S.F., Chen, H.L., Li, Z.L., Li, J.L., Sun, S., 2008. Middle Cambrian to Permian subduction-related accretionary orogenesis of Northern Xinjiang, NW China: implications for the tectonic evolution of central Asia. Journal of Asian Earth Sciences 32, 102–117.

Xiao, W., Windley, B.F., Allen, M.B., Han, C., in press. Paleozoic multiple accretionary and collisional tectonics of the Chinese Tianshan orogenic collage. Gondwana Research, http://dx.doi.org/10.1016/j.gr.2012.1001.1012.

Xiao, W.J., Windley, B.F., Badarch, G., Sun, S., Li, J., Qin, K., Wang, Z., 2004. Palaeozoic accretionary and convergent tectonics of the southern Altaids: implications for the growth of Central Asia. Journal of the Geological Society 161, 339–342.

Xiao, W.J., Windley, B.F., Yuan, C., Sun, M., Han, C.M., Lin, S.F., Chen, H.L., Yan, Q.R., Liu, D.Y., Qin, K.Z., Li, J.L., Sun, S., 2009. Paleozoic multiple subduction–accretion processes of the Southern Altaids. American Journal of Science 309, 221–270.

Xiong, X.L., Cai, Z.Y., Niu, H.C., Chen, Y.B., Wang, Q., Zhao, Z.H., Wu, J.H., 2005. The latePaleozoicadakites in eastern Tianshan area and their metallogenetic significance. Acta Petrologica Sinica 21, 967–976 (in Chinese with English abstract).

Xu, X.Y., Li, X.M., Ma, Z.P., Xia, L.Q., Xia, Z.C., Peng, S.X., 2006. LA–ICPMS zircon U–Pb dating of gabbro from the Bayingou Ophiolite in the northern Tianshan Mountains. Acta Geologica Sinica 80, 1168–1176 (in Chinese with English abstract).

Xu, Y.G., Lan, J.B., Yang, Q.J., Huang, X.L., Qiu, H.N., 2008. Eocene break-off of the Neo-Tethyan slab as inferred from intraplate-type mafic dykes in the Gaoligong orogenic belt, eastern Tibet. Chemical Geology 255, 439–453.

Xue, Y.X., Zhu, Y.F., 2009. Zircon SHRIMP chronology and geochemistry of the Haladala gabbro in south-western Tianshan Mountains. Acta Petrologica Sinica 25, 1353–1363 (in Chinese with English abstract).

Yang, J.S., Xu, X.Z., Li, T.F., Chen, S.Y., Ren, Y.F., Li, J.G., Liu, Z., 2011. U–Pb ages of zircons from ophiolite and related rocks in the Kumishi region at the southern margin of Middle Tianshan, Xinjiang: evidence of Early Paleozoic oceanic basin. Acta Petrologica Sinica 27, 77–95 (in Chinese with English abstract).

Yang, T.N., Li, J.Y., Sun, G.H., Wang, Y.B., 2006. Earlier Devonian active continental arc in Central Tianshan: evidence of geochemical analyses and Zircon SHRIMP dating on mylonitized granitic rock. Acta Petrologica Sinica 22, 41–48 (in Chinese with English abstract).

Yuan, C., Sun, M., Wilde, S., Xiao, W., Xu, Y., Long, X., Zhao, G., 2010. Post-collisional plutons in the Balikun area, East Chinese Tianshan: evolving magmatism in response to extension and slab break-off. Lithos 119, 269–288.

Zhou, M.F., Michael Lesher, C., Yang, Z.G., Li, J.W., Sun, M., 2004. Geochemistry and petrogenesis of 270 Ma Ni–Cu–(PGE) sulfide-bearing mafic intrusions in the Huangshan district, eastern Xinjiang, northwest China: implications for the tectonic evolution of the Central Asian orogenic belt. Chemical Geology 209, 233–257.

Zhou, M.F., Robinson, P.T., Malpas, J., Li, Z.J., 1996. Podiform chromitites from the Luobusa ophiolite (Southern Tibet): implications for melt–mantle interaction and chromite segregation in the upper mantle. Journal of Petrology 37, 3–21.

Zhou, M.F., Zhao, J.H., Jiang, C.Y., Gao, J.F., Wang, W., Yang, S.H., 2009. OIB-like, heterogeneous mantle sources of Permian basaltic magmatism in the western Tarim Basin, NW China: implications for a possible Permian large igneous province. Lithos 113, 583–594.

Zhou, M.F., Zhao, J.-H., Xia, X., Sun, W.H., Yan, D.P., 2007. Comment on "Revisiting the "Yanbian Terrane": implications for Neoproterozoic tectonic evolution of the western Yangtze Block, South China" [Precambrian Res. 151 (2006) 14–30]. Precambrian Research 155, 313–317.

Zhu, Y.F., Guo, X., Song, B., Zang, L.F., Gu, L.B., 2009. Petrology, Sr–Nd–Hf isotopic geochemistry and zircon chronology of the Late Palaeozoic volcanic rocks in the southwestern Tianshan Mountains, Xinjiang, NW China. Journal of the Geological Society 166, 1085–1099.

Zhu, Y.F., Guo, X., Zhou, J., 2006. Petrology and geochemistry of a $+\varepsilon$Nd gabbro body in Baluntai region, central Tianshan Mountains, Xinjiang. Acta Petrologica Sinica 22, 1178–1192 (in Chinese with English abstract).

Zhu, Y.F., Zhang, L.F., Gu, L.B., Guo, X., Zhou, J.B., 2005. The zircon SHRIMP chronology and trace element geochemistry of the Carboniferous volcanic rocks in western Tianshan Mountains. Chinese Science Bulletin 50, 2201–2212.

Zhu, Z.M., Zhao, Z.H., Xiong, X.L., Han, J.W., 2010. Petrogeochemistry of Late Paleozoic gabbroic rocks from Tekes County in West Tianshan Mountains. Acta Petrologica et Mineralogica 29, 675–690 (in Chinese with English abstract).